NAVAL POSTGRADUATE SCHOOL
Monterey, California

DTIC
S ELECTE
FEB 18 1992
D D

THESIS

EFFECT OF ALUMINA PARTICLE ADDITIONS ON
THE AGING KINETICS OF 2014-ALUMINUM MATRIX
COMPOSITES

by

Christopher Paul Harper (PE)

SEPTEMBER 1991

Thesis Advisor: I. Dutta

Approved for public release: Distribution is unlimited

92-03714

92 2 ⸱⸱ 176

SECURITY CLASSIFICATION OF THIS PAGE

REPORT DOCUMENTATION PAGE

1a. REPORT SECURITY CLASSIFICATION Unclassified		1b. RESTRICTIVE MARKINGS
2a. SECURITY CLASSIFICATION AUTHORITY		3. DISTRIBUTION/AVAILABILITY OF REPORT Approved for public release: Distribution is unlimited
2b. DECLASSIFICATION/DOWNGRADING SCHEDULE		
4. PERFORMING ORGANIZATION REPORT NUMBER(S)		5. MONITORING ORGANIZATION REPORT NUMBER(S)

6a. NAME OF PERFORMING ORGANIZATION Naval Postgraduate School	6b. OFFICE SYMBOL (If applicable) ME	7a. NAME OF MONITORING ORGANIZATION Naval Postgraduate School
6c. ADDRESS (City, State and ZIP Code) Monterey, CA 93943-5000		7b. ADDRESS (City, State, and ZIP Code) Monterey, CA 93943-5000
8a. NAME OF FUNDING/SPONSORING ORGANIZATION	8b. OFFICE SYMBOL (If applicable)	9. PROCUREMENT INSTRUMENT IDENTIFICATION NUMBER

8c. ADDRESS (City, State, and ZIP Code)	10. SOURCE OF FUNDING NUMBER			
	PROGRAM ELEMENT NO.	PROJECT NO.	TASK NO.	WORK UNIT ACCESSION NO.

11. TITLE (Include Security Classification)

EFFECT OF ALUMINA PARTICLE ADDITIONS ON THE AGING KINETICS OF 2014-ALUMINUM MATRIX COMPOSITES

12. PERSONAL AUTHORS
CHRISTOPHER PAUL HARPER (PE)

13a. TYPE OF REPORT Master's Thesis	13b. TIME COVERED FROM_____ TO_____	14. DATE OF REPORT (Year, Month, Day) SEPTEMBER 1991	15. PAGE COUNT 84

16. SUPPLEMENTARY NOTATION
The views expressed are those of the author and do not reflect the official policy or position of the Department of Defense or the U.S. Government

17. COSATI CODES			18. SUBJECT TERMS (Continue on reverse if necessary and identify by block numbers) aluminum matrix composites
FIELD	GROUP	SUB-GROUP	

19. ABSTRACT (Continue on reverse if necessary and identify by block numbers)

Differential Scanning Calorimetry (DSC) was conducted on 2014 aluminum, 2014 aluminum reinforced with 10 and 15 percent by volume of alumina particles, 2024 aluminum, and a Al/4%Cu alloy. Electrical resistivity and matrix micro-hardness measurements were conducted on the 2014 aluminum alloy and the metal matrix composites (MMC) during isothermal aging. Transmission Electron Microscopy (TEM) and DSC were used to identify the metastable phases formed in the 2014 aluminum alloy. The effect of alumina particle additions on the precipitation, growth and thermal stability of the metastable phases in the 2014 aluminum alloy and MMC were studied. Results were used to characterize the effect of the alumina reinforcement on the aging kinetics of the 2014 aluminum alloy matrix.

20. DISTRIBUTION/AVAILABILITY OF ABSTRACT XX UNCLASSIFIED/UNLIMITED __ SAME AS RPT __ DTIC USERS	21. ABSTRACT SECURITY CLASSIFICATION unclassified
22a. NAME OF RESPONSIBLE INDIVIDUAL I. Dutta	22b. TELEPHONE (Include Area Code) (408) 646-2581 · 22c. OFFICE SYMBOL ME/Du

DD Form 1473, JUN 86   Previous editions are obsolete.   SECURITY CLASSIFICATION OF THIS PAGE

S/N 0102-LF-014-6603   Unclassified

Effect of Alumina Particle Additions on the
Aging Kinetics of 2014-Aluminum Matrix Composites

by

Christopher Paul Harper (PE)
Lieutenant, United States Navy
BSME, University of Evansville, 1983

Submitted in partial fulfillment of the
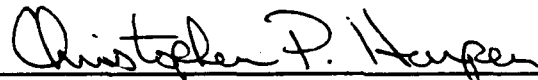requirements for the degree of

MASTER OF SCIENCE IN
MECHANICAL ENGINEERING

from the

NAVAL POSTGRADUATE SCHOOL

SEPTEMBER 1991

Author: _____
Christopher Paul Harper (PE)

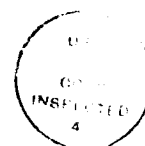Approved by: _____
I. Dutta, Thesis Advisor

_____
A.J. Healey, Chairman
Department of Mechanical Engineering

ii

ABSTRACT

Differential Scanning Calorimetry (DSC) was conducted on 2014 aluminum, 2014 aluminum reinforced with 10 and 15 percent by volume of alumina particles, 2024 aluminum, and a Al/4%Cu alloy. Electrical resistivity and matrix micro-hardness measurements were conducted on the 2014 aluminum alloy and the metal matrix composites (MMC) during isothermal aging. Transmission Electron Microscopy (TEM) and DSC were used to identify the metastable phases formed in the 2014 aluminum alloy. The effect of alumina particle additions on the precipitation, growth and thermal stability of the metastable phases in the 2014 aluminum alloy and MMC were studied. Results were used to characterize the effect of the alumina reinforcement on the aging kinetics of the 2014 aluminum alloy matrix.

iii

TABLE OF CONTENTS

LIST OF TABLES

vi

LIST OF FIGURES

viii

I. INTRODUCTION

A. METAL MATRIX COMPOSITES

Modern day design engineers are placing increased demands on engineering materials. New materials which provide high strength, low weight, thermal stability and ease of fabrication at a reasonable cost are required to meet these new demands. The striking improvement in material properties that can be obtained with metal matrix composites have made them attractive candidates.

Metal matrix composites (MMC) are a class of man made material which combine metallic properties such as ductility and toughness with ceramic properties like high stiffness and high temperature stability leading to greater strength, stiffness, higher operating temperatures and a host of other enhanced properties of the composite. The properties of an MMC can be tailor made to fit many service requirements.

MMCs are composed of a combination of a metallic matrix in which a nonmetallic reinforcement, usually a ceramic, is added to form a two phase mixture. Typical reinforcements include graphite fibers and whiskers, boron fibers, boron carbide, silicon carbide and aluminum oxide particles. Reinforcements can be in the shape of; continuous fibers with diameters as varied as 3μm to 200μm, whiskers with diameters of less than a 1μm and

irregular shaped particles with diameters of 3μm to 200μm. The continuous fibers offer the best improvement in stiffness and strength when measured along the fiber axis yet they exhibit the most anisotropic properties and are nearly impossible to manufacture into intricate shapes. The irregular shaped particles offer the most isotropic conditions and are generally the easiest to manufacture in intricate patterns yet offer the least improvement in stiffness and strength of all MMCs.

Until recent advances in the manufacture of discontinuous reinforced MMCs, the traditional method of fabrication was by powder metallurgy (PM) techniques. These techniques are rather expensive, time consuming and because of the high pressures required, product size is limited. Recent advances in casting of MMCs have overcome the majority of manufacturing problems and has opened the door to good quality, low cost MMCs with a wider availability of product size and shape.

Because of the ease of fabrication with conventional equipment and the resultant lower cost, the particulate reinforced metal matrix composite, made by ingot casting techniques, is finding increased use in the aerospace, automotive, military and sporting good industries [Refs. 1, 2]. The choice of reinforcement and matrix used to produce the MMC is paramount to producing a composite with the desired properties. With the choices available, it becomes important to understand how the reinforcement affects the microstructural development of the matrix material as well as the overall properties of the

MMC. This has resulted in the need for further research on these materials. Of particular interest here are the effects of the reinforcement on the ageing behavior of the material with resultant effects on microstructural characteristics and mechanical properties.

B. MICROSTRUCTURAL EVOLUTION IN THE 2014 ALUMINUM ALLOY

Aluminum alloy 2014 is an age hardenable alloy with the nominal composition shown in Table I [Ref. 3]. The major constituents (Al, Cu, Si, Mg) allow for the possible following precipitation sequences:

$$\theta'' - \theta' - \theta \qquad (CuAl_2)$$

$$sss - GP - GPB + GP - \quad S' - S \qquad (CuMgAl_2)$$

$$\beta' - \beta \qquad (Mg_2Si)$$
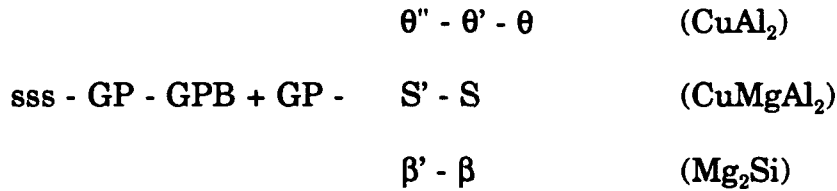
TABLE I. COMPOSITION OF 2014 Al ALLOY

Cu	Si	Mg	Mn	Fe	Zn	Cr	Ti
3.9 to 5.0	.5 to 1.2	.2 to 03	.4 to 1.2	.7 max	.25 max	.10 max	.15 max

Many studies [Refs. 4, 5, 6] have suggested θ and S phase precipitates in the aged alloy with some identification provided by transmission electron microscopy (TEM) and differential scanning calorimetry (DSC). The β phase has not been positively identified in any available literature but has been

3

suggested as the precipitation sequence most probable when aged in the temperature range (27°C to 130°C) [Ref. 7].

Singh and Goel [Ref. 8] studied the influence of thermomechanical aging (TMA) on the mechanical properties of 2014 aluminum. In their work they subjected their samples to varying degrees of warm rolling and then determined mechanical properties of the material by tensile tests. Electron microscopic studies revealed that TMA treatments substantially affected the aging characteristics. Singh & Goel stated that the strengthening effects in 2014 aluminum alloy may be considered to be due to; 1) Coherent precipitate θ'', 2) Partially coherent precipitate θ', and 3) the dislocation substructure. They determined that the increase in strength due to thermal aging after mechanical treatment is attributed to the semicoherent θ' precipitate.

It is known that the dislocation substructure controls the precipitate size, shape and distribution. The heterogeneous nucleation of θ' precipitate is enhanced by the presence of dislocations; therefore the strength will be high when fine θ' particles are formed in a dense dislocation matrix structure.

Further observation from Ref. 8 is that no θ'' was identified in any worked sample at any aging temperature, although it was observed in the samples with no prior deformation history. From this Singh concluded that with an increase in the dislocation density, θ' is preferentially nucleated over θ''.

Patterson and Sheppard [Ref. 9] investigated the structural changes that occur during thermal treatment of a 2014 aluminum alloy. Samples exposed

to a 1 hour 500°C soak were artificially aged with micro-hardness readings taken periodically. TEM micrographs were taken at peak hardness in an attempt to identify the microstructure. At peak hardness at all aging temperatures, θ'' plates with large strain fields were the main precipitate identified, although some θ' plates with very small strain fields could also be found. The optimum aging temperature was determined to be 160°C with peak aging occurring in 18 hours. At the lower aging temperature of 120°C, microstructural changes were very slow (peak hardness after 720 hours) they surmised that this behavior suggests that the early stages of aging are dominated by formation of GP1 and GPB zones and that nucleation of θ' & θ'' does not occur until the later stages. Aging at 180°C resulted in quite rapid overaging suggesting that the higher temperatures promote transition of GP1 zones to θ'' and accelerates θ' precipitation.

Paterson and Sheppard suggest that the early strength increase prior to θ' and θ'' appearing in the matrix may be attributed to the formation of GP1 and GPB zones which act as obstacles to dislocation motion. However no GPB zones or S type precipitates were identified anywhere in this work.

In the work done by Gronostajski and Tobota [Ref. 10], thermomechanical treatment of a 2014 aluminum alloy was used to investigate the microstructure at peak hardness. After cold working, solutionizing and aging the alloy, they identified only the θ' precipitate in the microstructure. No GP zones or θ'' were found. They concluded that deformation, and the resultant increase in

5

dislocation density, accelerated the precipitation of the θ' phase, as a result of the extra nucleation sites in the matrix. S type precipitates were also absent from this investigation.

Abis and Riontino [Ref. 4] in their work on aluminum alloys predicted that the precipitation sequence for 2014 aluminum alloy should be:

$$\theta'' - \theta' - \theta \qquad\qquad CuAl_2$$
$$sss - GP - GPB + GP - \quad S' - S \qquad\qquad CuMgAl_2$$
$$\beta' - \beta \qquad\qquad Mg_2Si$$
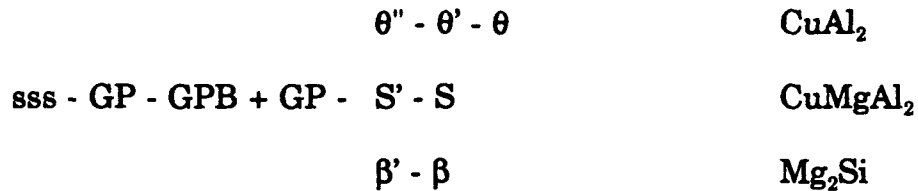
They go on to predict that the relative amounts of Mg and Si excludes the presence of the β phase in this alloy.

Abis and Riontino performed a DSC trace on a 2014 sample solutionized and quenched with the following results; An exothermic peak centered at 60°C which they assign to GPB & GP1 precipitation, a wide endothermic peak approximately 120°C wide centered at approximately 160°C which is assigned the dissolution of GP1 & GPB precipitates, two narrow, large exothermic peaks centered at 220°C and 270°C were assigned to θ' and S' precipitation. Finally a large endothermic peak commencing at 340°C which they suggest signifies the dissolution of all precipitates.

Datta and Bonfield [Ref. 11] investigated the precipitation hardening in an Al, 4%Cu, .8%Mg, .8%Si, .7%Mn, .5%Fe (2014) alloy. They found that the precipitation sequence varied with the aging temperature. At low aging temperatures (130°C) the hardness-time plots had intermediate plateaus which

6

they ascribed to the sequential precipitation of GP zones, θ" and θ' precipitates. The peak hardness at this aging temperature was reached after 100 hours of aging. No apparent overaging occurred during this test period which spanned 1000 hours. No microstructural changes were noted until 80 hours of aging when θ" precipitates, with extensive strain fields were first identified. Faint <100> matrix spot streaking was also obtained in the selected area diffraction pattern (SADP) at this time. θ' precipitate along with its diffraction spots was positively identified by TEM, SADP after 150 hours of aging at 130°C.

At an intermediate aging temperature of 160°C the hardness curve flattened out after about 10 hours with peak hardness reached after 40 hours of aging. Peak hardness was maintained until a sudden drop at approximately 200 hours of aging, signifying a long incubation time prior to overaging. At an aging temperature of 190°C peak hardness was reached after 4 hours with overaging occurring after about 20 hours.

At both 160 and 190°C aging temperatures the onset of <100> streaking of the {200} matrix spots was observed (1 hour) prior to θ" precipitation (2 hours). θ' precipitate diffraction spots were identified after 3 hours. They attribute the slow overaging at these temperatures to the slow measured growth rate of θ' particles and the consequent retention of coherency strain.

Peak hardness when aging at 130°C was attributed to relatively equal amounts of θ' and θ" precipitate in the matrix. Peak hardness for 160°C and 190°C aging temperatures was attributed to semicoherent θ' precipitates alone.

7

These results would suggest that θ'' precipitate tends *to* transform to θ relatively quickly and/or θ' precipitates vice θ'' at these elevated aging temperatures.

It is interesting to note that during this testing no evidence of S' or S precipitates were identified at any aging temperature. The "major aging sequence" proposed for this alloy is:

$$sss - GP1 \text{ zones} - \theta'' - \theta'$$

However, this sequence does not account for the great increase in hardness exhibited during the first hour at the intermediate and elevated aging temperatures and the first 80 hours of aging at 130°C, since no matrix spot streaking in the <100> direction or other evidence of this phase sequence was noted. This increase in hardness may be related to the precipitation of GPB zones (Al-Cu-Mg) which produce smaller lattice strains than GP1 zones.

Silcock [Ref. 12] investigated a Al-Cu-Mg alloy with an 7:1 Cu:Mg ratio. She observed the presence of both GPB and GP1 zones together and upon continued aging these zones were succeeded by θ'', θ' and S' precipitates. She also noted that GPB precipitates were still observable at and after peak hardness at the 130°C, 190°C and 240°C aging temperatures. Based on these reports the evidence would suggest that the GPB zones persist throughout the aging sequence at these temperatures, and both the S $(CuMgAl_2)$ and θ $(CuAl_2)$ phase sequences are present in this alloy.

8

In a follow on to their earlier study Datta and Bonfield [Ref. 5] investigated the zone formation during room temperature aging of a Al-4%Cu-.8%Si-.8%Mg alloy. They found that the precipitation hardening was associated almost entirely with the formation of GPB type zones. Peak hardness was reached after 48 hours of aging with no further change for the remaining duration of the test (1000 hours). The selected area diffraction patterns (SADP) performed on the sample at peak hardness did not reveal either the characteristic <100> streaking associated with GP1 formation or any evidence of θ'', θ' or S' precipitates. These results caused Datta and Bonfield to postulate that the hardening sequence for room temperature aging was associated with GPB zone formation. This correlates with investigations by Silcock [Ref. 12] and Wilson [Ref. 6] who have determined that the GPB type zones produce only small lattice strains which are not observable by SADP.

Datta and Bonfield demonstrated that at room temperature, for this alloy concentration, 94% of all vacancies should be associated with Si atoms and only 6% with (Cu + Mg). They concluded that the silicon atom vacancy association contributed to the zone formation during aging, with a resultant GPB type zone of Al-Si-(Cu-Mg) vice a GP1 (Al-Cu) zone. Since the vacancy partitioning is both concentration dependent and temperature dependent, as the concentration of other constituents increases relative to the Si concentration or as the aging temperature goes up the effect of Si vacancy

9

clustering will decrease, with a corresponding increase in the precipitation of GP1 (Al-Cu) zones and GPB (Al-Cu-Mg) zones.

From the results of their work it was concluded that the transformation from GPB zones to S' precipitates was favored at an aging temperature between room temperature and 130°C, for this alloy.

Wilson [Ref. 6] set out to determine the effects of small additions of silicon to a Al- 2.5%Cu- 1.2%Mg alloy. He found that the addition of amounts as small as .24% Si had a significant effect on the precipitation hardening of the alloy, affecting all stages in the precipitation sequence.

Examination of the silicon free alloy showed that aging below 190°C produced a high density of dislocation loops and helical dislocations by vacancy condensation. These loops became fewer and larger as the aging temperature increased. S' precipitates were determined to heterogeneously nucleate at dislocations and were partially incoherent with the matrix throughout their growth.

Examination of the alloy with .24% Si addition while aging in the 100°C to 300°C range showed almost a complete absence of vacancy loops even after prolonged aging. At artificial aging temperatures in the 100°C to 300°C range S' precipitates formed rapidly by nucleating throughout the matrix. A homogeneous distribution of GPB and S' precipitates were observed at peak hardness (16 hours at 190°C). This microstructure was very similar to the microstructure obtained at peak hardness for a sample aged at 300°C for 5

minutes. Wilson suggests that the addition of silicon raised the GPB zone solvus temperature from 190°C to above 300°C in this alloy. Weatherly, as reported by Wilson, had produced similar evidence for the transformation of GPB zones to S' precipitates at 190°C in a similar Si free alloy. Wilson concluded that the effect of silicon was to increase the effective binding energy between the solute atoms, vacancies and GPB zones, enhancing the stability of the zones and raising the temperature at which the S' precipitates form by transformation from GPB zones.

Radmilovic *et al.* [Ref. 13] studied the nucleation and growth of the transition $CuMgAl_2$ (S') precipitate in the Al-Cu-Mg and Al-Cu-Mg-Li systems. In the Al-Cu-Mg-Li system Radmilovic found that S' nucleated directly from the matrix by two methods: nucleation of S' on matrix dislocations followed by growth of rod-like and plate-like S' with a <102> habit plane and, secondly during the growth of $Al_3Li(\delta')$ excess Cu and Mg atoms cluster at the growth front. This coupled with the vacancies released from the Li/vacancy clusters, when Li combines in the $Al_3Li(\delta')$ phase resulted in S' nucleation.

In the Al-Cu-Mg alloy S' was found to nucleate on subgrain and grain boundaries. S' was also noted to transform from clusters of Cu-Mg rich regions which were identified as GPB zones.

From Radmilovic's work it is possible to predict the following possible modes of formation of the S phases in the 2014 Al alloy; GPB zone formation by the clustering of Cu and Mg, S' formation by the heterogeneous nucleation

11

at interfaces like grain boundaries or growth fronts, and transformation from GPB zones.

Rosen and Horowitz [Ref. 14] investigated the aging kinetics of aluminum alloy 2024. They determined that two distinct precipitation sequences were taking place in the 0°C to 70°C aging range. They identified these two precipitates as the GP1 (Al-Cu) zones and the GPB (Al-Cu-Mg) zones. At aging temperatures above 100°C, they found intermediate precipitates, predominantly S', formed vice the GP1 and GPB zones. A small amount of θ ($CuAl_2$) and S ($CuMgAl_2$) were identified along the grain boundaries.

During hardness testing Rosen and Horowitz found that the majority of the increase in hardness was attributed to the GP1 and GPB zone formation. They found only a small increase in the hardness was due to the θ' and S' precipitates.

During electrical resistance measurements, the maximum resistance was determined to be after 60 hours when aged at 180°C. The maximum hardness was found to be after 16 hours when aged at this same temperature. This correlates with other investigations [Ref. 15, 16] and is the result of differing relative mechanical and electrical resistances between GP, GPB zones and θ, S precipitates.

Rosen and Horowitz also studied the effect of an increased dislocation density on the reaction kinetics of their alloy. They mechanically deformed their specimen to create a homogeneous distribution of dislocations. They found

12

that the increased number of dislocations provided additional nucleation sites for precipitation and caused the initial electrical resistivity change to be larger. Additionally the hardness measurements showed a fixed increase over the whole range of aging.

Conserva *et al.* [Ref. 17] in their paper on structural hardening processes in Al, (4-5)% Cu, (.3-.8)% Mg, (.5-1.2)% Si systems, predicted that the first stages of aging are characterized by three types of zone formation: the $CuAl_2(\theta)$ GP zone, the $Mg_2Si(\beta)$ GP zone and the $CuMgAl_2(S)$ GPB zone. They hypothesized that Mg_2Si zones should be the first to form if the Mg:Si ratio is greater or equal to 1.73 since these two elements share a great chemical affinity. They also predict for Cu/Mg ratios of 5 to 7 both GP zones and GPB zones should form. They proposed the following aging sequence for the alloy:

$$\theta" - \theta' - \theta \qquad (CuAl_2)$$

sss - GP1 ($CuAl_2 + Mg_2Si$) + GPB - $\quad S' - S \qquad (CuMgAl_2)$

$$GP\ ord.- \beta' - \beta \qquad (Mg_2Si)$$
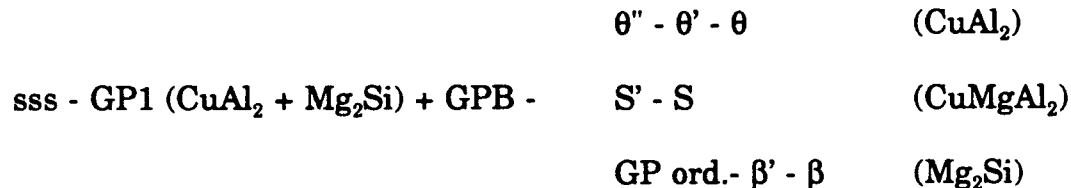
This agrees with the aging sequence proposed by Abis and Riontino for the general aging sequences for Al, Cu, Mg, Si systems.

Brandt *et al.* [Ref. 18] examined the precipitation sequence in Al-Cu-Li-Mg alloys. They sought to determine if the sequence could be considered to consist of the independent precipitation of δ'(Al-Li) and S'(Al-Cu-Mg). They confirmed the existence of both precipitation sequences by transmission

13

electron microscopy (TEM), however interaction between these phase sequences was observed by differential scanning calorimetry (DSC).

DSC results on a sample of Al-2.8Li were analyzed and are characterized as follows; an exothermic peak at 150°C was assigned to precipitation of δ', an endothermic peak at 290°C assigned to the dissolution of δ' and an exothermic peak centered at 300°C the precipitation of δ. DSC results on a sample of Al-4.7%Cu-1.9%Mg are characterized as follows: an endothermic peak between 150°C and 250°C was assigned the dissolution of previously formed GPB zones and an exothermic peak at 280°C which is assigned the precipitation of S'. The Al-Cu-Mg alloy also exhibited a possible endothermic peak starting at 320°C which could be the dissolution of the S'. The Al-Li DSC trace was algebraically summed to the DSC trace for the Al-Cu-Mg alloy. This theoretically obtained curve was then compared with the DSC curve of a sample containing Al-4.4 Cu-2.8 Li-1.7 Mg. From this comparison it was observed that the precipitation process in Al-Cu-Mg-Li was not a simple addition of the two separate precipitation processes attributed to the Al-Li and Al-Cu-Mg systems. The lithium addition interacted with the Al-Cu-Mg (GPB) and (S') precipitation sequences. However transmission electron microscopy (TEM) of the Al-Cu-Li-Mg sample resulted in the independent observation of both δ'(Al-Li) and S'(Al-Cu-Mg) precipitates.

From the results of the previously discussed work it is obvious that a consensus on the sequence of precipitation and the phases that form during

14

aging of the aluminum alloy 2014 has not been reached. An independent analysis of the individual alloying elements would suggest the formation of the β phase (Mg_2Si) the S phase ($CuMgAl_2$) and the θ phase ($CuAl_2$). From the results of Brandt et al. [Ref. 18] we should conclude that all 3 phases are formed although to what extent they interact with one another is not determined. Results from other research suggest that the interaction between the independent alloys are quite different than the sum of the phases and can result in the retardation of some of the precipitation phases.Some of the reviewed papers positively identified both θ', θ" of the $CuAl_2$ phase sequence and S' of the $CuMgAl_2$ phase sequence in the 2014 alloy. Other research suggests the formation of GPB zones of the Al-Cu-Mg phase sequence dominates the early stages of aging. These GPB zones were hypothesized to form at low temperature aging (ambient to 100°C) and may remain stable up to 300°C.

C.   ACCELERATED AGING IN METAL MATRIX COMPOSITES

Composite materials are characterized by two or more dissimilar phases. The properties of these two phases vary significantly, yet they must be compatible with one another to form a material with the desired characteristics. A known effect of adding a ceramic reinforcement to a aluminum matrix is a significant change in the base metals precipitation hardening characteristics. There are two primary theories to explain the

mechanism of accelerated aging in MMC's [Refs. 19, 20, 21]. Both mechanisms can be attributed to the thermal mismatch strain between the reinforcement and the matrix. This strain is a function of the difference in the coefficients of thermal expansion between the matrix and the reinforcement and the change in temperature from the low strain composite condition.

The first theory that explains accelerated aging is that the strain fields generated by the thermal expansion mismatch are relaxed by the formation of a dislocation network in the matrix. These dislocations serve as additional nucleation sites for second phase precipitation. With the number of nucleation sites greatly enhanced the precipitation of second phase particles will also be enhanced. Since the operating mechanism for this theory is the thermal expansion mismatch, the larger the mismatch the more pronounced the accelerated aging should be.

The second theory to explain accelerated aging in the composite is that the stress fields generated by the thermal expansion mismatch, enhances the diffusion paths of the solute atoms through the matrix. Since these solute atoms tend to migrate to common areas in the matrix the enhanced concentration of solute atoms in these regions promote the nucleation and growth of second phases.

Dutta and Bourell [Ref. 21] studied an aluminum alloy reinforced with 10 vol% SiC whiskers of variable aspect ratios in an attempt to identify the operating mechanism for accelerated ageing in MMC's. They predicted that

this mechanism depended on several factors, including the size and volume fraction of the reinforcement. For larger fiber radii (1µm min.) and high dislocation density ($10-14/m^2$ min.) the dislocation mechanism should dominate. For smaller radii (.25µm max.) and lower dislocation density ($10-13/m^2$ max.) the solute atom diffusion mechanism should dominate. For fiber radii of (.25µm to 1µm) both mechanisms were expected to contribute.

Experimental results of tests on a composite that should have exhibited both mechanisms found that the dislocation mechanism dominated. They hypothesized that the local stress field of a dislocation overwhelmed the long range stress field of the reinforcement resulting in solute atom attraction to the dislocations vice diffusion down the stress gradient generated by the reinforcement.

Dutta, Allen and Hafley [Ref. 16] studied the effects of Al_2O_3 particle reinforcement in a 6061 Al matrix. The effect of 10 and 15 vol% alumina particulate addition on the aging behavior was studied by differential scanning calorimetry (DSC), electrical resistivity, microhardness and transmission electron microscopy (TEM). They determined that the precipitation sequence was significantly accelerated in the composite due to the increased dislocation density. They also determined that the relative amounts of the various phases were also affected by the reinforcement addition. The dislocation density was measured for the monolith and compared to the 10 and 15 vol% Al_2O_3 composite in the as quenched condition by TEM. It was determined that the

dislocation density increased by two orders of magnitude in the composites when compared to the control alloy but the change in dislocation density varied little between the 10 and 15 vol% composites.

The increased dislocation density significantly increased the number of sites for nucleation resulting in a decrease in the incubation time for precipitate nucleation. Nucleation of precipitates was found to take place on two kinds of sites (1) Matrix dislocation and (2) Vacancy loops. As the reinforcement concentration increased the nucleation was more likely to occur on dislocations since the formation of the dislocations are at the expense of the vacancy concentration. Only nucleation on the matrix dislocations was found to be accelerated by the addition of reinforcements. This was evidenced by the constant peak temperature for silicon-vacancy clustering when varying reinforcement concentration on DSC testing.

The precipitate growth rate was found to be enhanced in the composite. The variation of electrical resistivity with aging indicated that the time to peak aging and overaging were accelerated in the composite. From this study, they determined that the presence of reinforcements increased the diffusion of the solute atoms, necessary for precipitate growth, by increasing the matrix dislocation density.

It was also observed that the relative amounts of the various phases were decreased when the alumina reinforcement was added. It was proposed that the increased dislocation density in the composite assisted the precipitation of

coherent precipitates in such an orientation as to reduce the overall strain energy. This would stabilize these coherent precipitates reducing the likelihood of their transformation into the semi-coherent and incoherent, usually more stable phases.

Papazian [Ref. 22] studied the effects of the addition of short SiC whiskers on the age hardening and precipitation sequence of 2124 and 2219 aluminum alloys made be powder metallurgy (PM).

Results of differential scanning calorimetry (DSC) testing of an 8% SiC and a 20% SiC-2124 composite were compared to the 2124 base alloy. Papazian found that the overall characteristics of the, S phase, age hardening kinetics were not significantly altered. The GPB peak temperature remained relatively constant showing a very slight increase with larger additions of reinforcement. As the reinforcement addition was increased the magnitude of the GPB peak decreased indicating reactions were less energetic in the composite material. This is indicative of less GPB zones forming in the composite material when compared to the monolith. The S' formation peak did not show any change in magnitude of peak temperature when comparing the composite to the monolith.

The results of DSC scans on a 20% SiC-2219 composite were compared to the 2219 base alloy where the θ phase sequence ($CuAl_2$) is the primary second phase formed. It was determined that the addition of SiC reduced the volume fraction of GP zones that precipitated, lowered the peak transformation

temperature of θ' by 40°C, indicating significant accelerated aging, and substantially increased the volume fraction of θ' formed.

Papazian proposed that the addition of the reinforcement to the matrix decreased the vacancy concentration due to the higher dislocation density. The lower vacancy concentration reduced the number of GP and GPB zones formed, since vacancies are preferred nucleation sites. The larger θ' zone was explained as a combination of more nucleation sites due to the enhanced dislocation density and the introduction of SiC-Al interfaces. Papazian also showed that aging was affected by the method used to form the composite. The two primary processing techniques used to manufacture metal matrix composites are powder metallurgy (PM) and ingot casting. When comparing the DSC scan for two similar materials with different manufacturing history, Papazian showed that the PM sample exhibited accelerated aging compared to the cast sample. Papazian further showed that the greatest portion of the accelerated aging in the composites were caused by the manufacturing technique and only a small portion of the overall effect of accelerated aging was caused by reinforcement addition.

Christman, Suresh and Sugimura [Ref. 23] studied the evolution of the microstructure in a cast Al-3.5 weight % Cu alloy reinforced with varying amounts of SiC particulate. Matrix microhardness was recorded for the monolithic alloy and the composites reinforced with 6, 13 and 20 vol% SiC particles while aging at 190°C. They found that all of the materials exhibited

20

essentially the same microhardness in the solutionized and quenched condition. This would suggest that the dislocation density, which increases with percent reinforcement, has in itself no measurable effect on the matrix strengthening.

Another result of Christman *et al.* study is that the composite material reached peak hardness in approximately one third the time it took for the control alloy to reach peak. This demonstrates that this material, Al-3.5% Cu, with its precipitate θ phase sequence does exhibit accelerated aging due to the reinforcement addition. It was impossible from the test data to determine the effects of varying amounts of reinforcement on peak hardness or on time to peak hardness however, because of the large data scatter in the microhardness readings. From their results, they determined that the extent of accelerated aging is relatively insensitive to the volume fraction of the reinforcement, for this alloy and reinforcement combination.

Christman and Suresh [Ref. 24] studied the microstructural development in an 2124 aluminum alloy with and without an addition of 13.2 vol% SiC whisker reinforcement. They found the matrix of the composite material had a much higher density of dislocations than the control alloy and these dislocations were fairly uniform in distribution. The composite material exhibited accelerated aging with peak hardness of the composite reached in a third of the time of the monolith. Transmission Electron Microscope (TEM) micrographs found the incubation time of the S' phase to be approximately one hour in the composite compared to a four hour incubation time in the monolith.

The rate of decrease in conductivity of the composite with aging was almost twice as fast as that of the monolith in the early stages of aging. TEM micrographs showed the S' phase tended to nucleate on dislocations during the initial stages of aging and grew into corrugated sheets in the overaged microstructure.

Christman and Suresh predicted and showed by TEM that upon solutionizing and quenching the composite, dislocations are punched out from the whisker ends, and since they can travel up to the length of the whisker, the dislocation density is fairly homogeneous. This high density, uniform distribution of dislocations in the composite serve as nucleation sites, enhancing the nucleation of the strengthening precipitates.

The matrix microhardness measurements demonstrated that while the peak hardness of the two materials were approximately equal, the time to peak for the composite was approximately one-third that of the monolith. The composite material showed an immediate increase in hardness with aging while the monolith was insensitive to artificial aging for the first two hours. The solutionized and quenched monolith was significantly harder than the composite material prior to aging.

TEM was used to determine the extent of dislocation generation in the composite and their effect on the precipitation kinetics of the material. TEM micrographs of the solutionized and quenched composite showed a high density of helical dislocation loops, indicative of vacancy condensation during

quenching. Studies of micrographs taken during the aging prior to peak showed that S' nucleation was taking place mainly on dislocations. Micrographs of the overaged condition showed the S' phase in the form of corrugated sheets throughout the matrix and the S phase mainly on the grain boundaries.

The dislocation density was extremely high in the composite compared with the monolith. This can be attributed to two factors, the large difference between the thermal expansion coefficients (about a factor of 10) between the Al matrix and the SiC reinforcement and the phenomenon of dislocation generation at the ends of the whiskers. Because the dislocations were fairly uniform in the matrix the precipitation hardening was identified throughout the matrix and not just near the reinforcement which may be the case for a smaller CTE mismatch and particulate vice whisker reinforcements.

From the literature reviewed and highlighted previously it is quite obvious that there are many factors which influence the aging kinetics of precipitation hardenable metal matrix composites.

Although it is generally agreed that there is two possible mechanisms for accelerated aging, there is not much of a consensus on which mode is operative in a given system. Dutta and Bourell [Ref. 21] showed that theory and observation do not necessarily coincide when predicting modes of accelerated aging.

Both of the proposed modes for accelerated aging are dependent on the CTE mismatch and the size and shape of the reinforcement. Therefore composites manufactured with the aluminum and SiC particles ($\Delta CTE=10$) should react quite differently than aluminum alloys reinforced with Al_2O_3 ($\Delta CTE=3$). Composite systems reinforced with whiskers are expected to have a much higher dislocation density, that are more homogeneously distributed, than systems with particulate reinforcement.

Accelerated aging is also dependent on the precipitation phase formed. From the research of Papazian [Ref. 22] it could be concluded that the S phase sequence ($CuMgAl_2$) does not exhibit accelerated aging, however Christman and Suresh [Ref. 24] found in their study that the S phase sequence does exhibit accelerated aging. Dutta, Allen, Hafley [Ref. 16] found that the β phase sequence does exhibit accelerated aging and Papazian [Ref. 22] found similar results for the θ phase sequence.

D.   RESEARCH OBJECTIVE

The effects of reinforcing 2014 aluminum (with its potential S, θ, β aging sequences) with alumina (Al_2O_3) reinforcement is not obvious from the previous discussions. Further detailed study in this area is required to determine if there is any effect of varying additions of alumina particles on the aging characteristics of the cast 2014 aluminum matrix.

The purpose of this present work is two part. First, to determine what metastable phases are formed in the 2014 aluminum alloy, and second, how the addition of 10 and 15 percent by volume alumina particle reinforcement affects the precipitation, growth and thermal stability of these metastable phases in the 2014 aluminum alloy, MMC.

II. DESCRIPTION OF MATERIALS

The metal matrix composite used in this study were fabricated using a proprietary casting technique developed by Dural Aluminum Composites Corporation, San Diego, California. In this patented process, the alumina particles, approximate size 15μm (15 vol%) and 6μm (10 vol%), are added to the molten aluminum while vigorously stirring. The alumina reinforcement is thoroughly wetted by the aluminum without significant chemical interaction. The composite is hot-extruded after casting to homogenize the microstructure. The matrix material and the 2014 Al alloy are commercial grade produced by ingot casting techniques.

There is a appreciable degree of clustering of alumina in the composite materials. This clustering is observable as bands of reinforcement in the 10 vol% composite (Figure 1). The 15 vol% composite shows much less clustering of reinforcement than the 10 vol% and the banding prevalent in the 10 vol% is not observable (Figure 2).
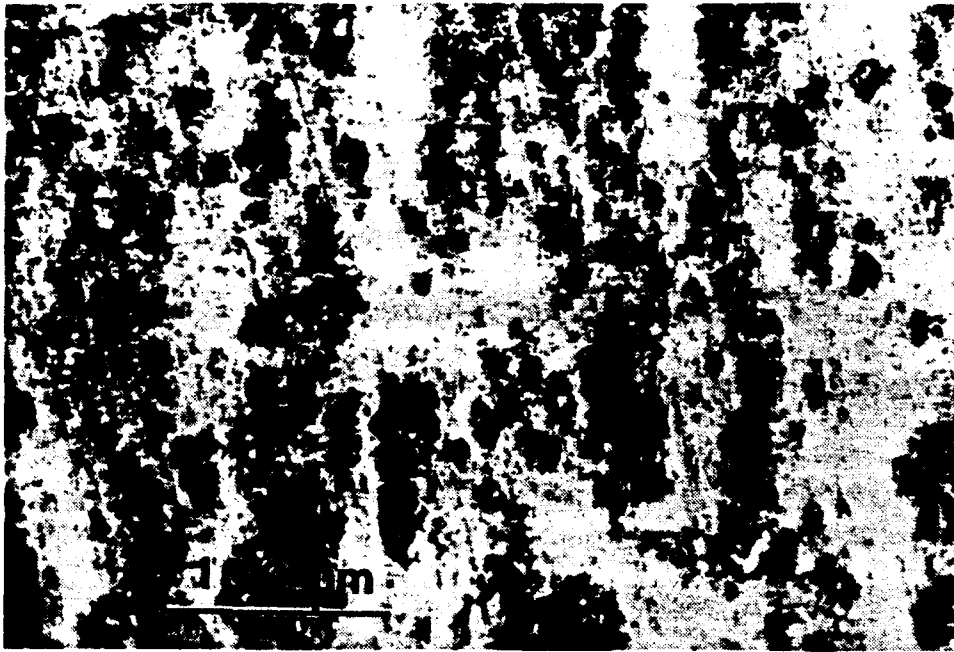
Figure 1: Micrograph of the 2014 Al alloy MMC with 10 vol% Al$_2$O$_3$ addition. The average size of the reinforcement in this MMC is 5 x 8μm.
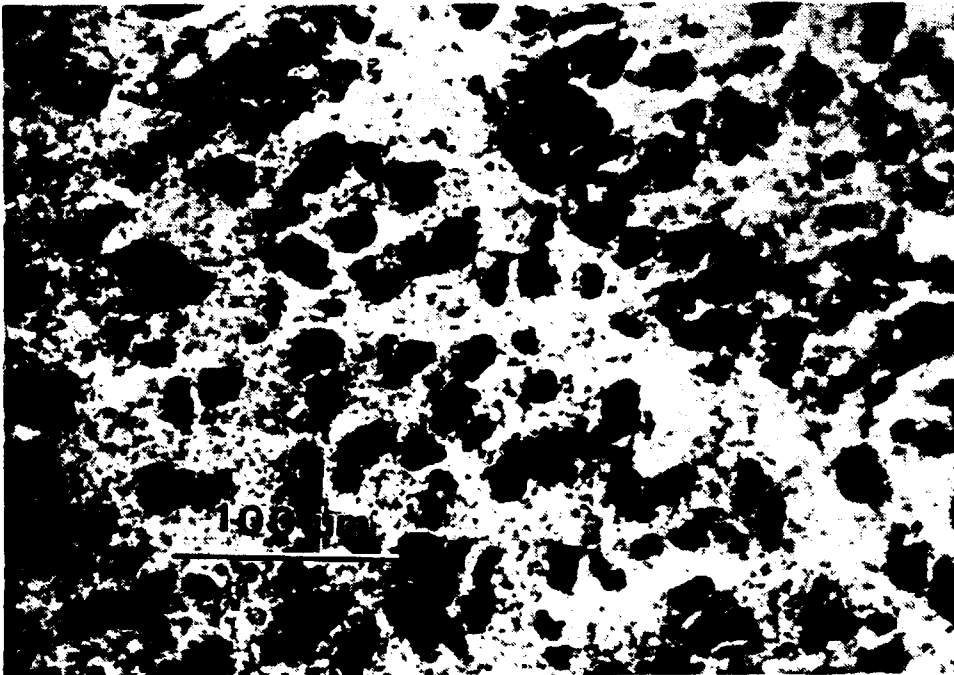
Figure 2: Micrograph of the 2014 Al alloy MMC with 15 vol% Al$_2$O$_3$ addition. The average size of the reinforcement in this MMC is 8 x 22μm.

III. EXPERIMENTAL PROCEDURE

A. RESISTIVITY

The changes in resistivity during isothermal aging of the 2014 Al alloy base material and the 2014 reinforced with 10 vol% and 15 vol% Al_2O_3 were recorded using the same test equipment as Hafley [Ref. 25] and Allen [Ref. 15]. Modifications to the test rig were accomplished to minimize data scatter and facilitate quick loading of samples. Quick loading of test samples is critical at elevated aging temperatures since the peak aged condition occurs within a matter of seconds.

Resistivity samples were cut to fit the test jig and had a final machined size of 115mm * 3.6mm * 1.8mm. Samples were solutionized in an argon purged atmosphere at approximately 535°C for 90 minutes. Formation of the supersaturated solid solution was insured by a rapid ice water quench from solutionizing temperature. The samples were immediately placed into the test jig which had been soaking in the isothermal aging oven already stabilized at the appropriate temperature. The change in resistivity was measured during isothermal aging at the following temperatures: 40°C, 100°C, 150°C, and 200°C. Data acquisition was performed with the aid of a desk top computer and Basic programs developed by Hafley [Ref. 25]. In all cases the data acquisition system was set to acquire data every second for the first two minutes and then

at intervals appropriate for the aging temperature for the remainder of the run.

B. HARDNESS TESTING

The precipitation hardening of the monolith 2014 Al alloy and the two corresponding MMCs were measured with the Buehler Micromet Vickers Microhardness Tester with 50 and 100 gram loads. All samples were cut to approximately the same size with the same thickness and care was taken to insure parallel faces. One face was polished with 1 micron alumina paste to ensure a smooth surface for the micro hardness readings. All samples were solutionized in a 535°C oven with an argon purge for 90 minutes and subsequently quenched in an ice water bath. The samples were artificially aged at 185°C for a sequence of times, removed and quenched in ice water to stop further aging. All samples were briefly polished to remove the oxide layer on the prepared face. An average of six hardness measurements were taken from each aged sample. Care was necessary to ensure the indentor was in contact with only the matrix material but was close enough to the reinforcement to measure the effects of the alumina addition. The results of the hardness measurements were converted to a Vickers hardness number for reporting purposes.

C. TRANSMISSION ELECTRON MICROSCOPY (TEM)

Samples for TEM examination were prepared from the monolithic 2014 Al alloy by slicing approximately .20mm thin foils on a low speed diamond saw with additional thinning by hand sanding. Disks 3mm in diameter were punched from the foil. Samples were solutionized at 535°C in an argon purged furnace for 90 minutes and ice water quenched. The samples were placed in the DSC and aged to approximately 5°C above each exothermic peak, and then immediately cooled at a rate approaching 320°C/minute in order to maintain the microstructure which developed at the required temperature. After the heat treatment, the samples were lightly sanded with 600 grit sandpaper, to remove the oxide layer, and then thinned by electro-polishing in a Struders Tenupol twin-jet system. The electro polish solution was composed of 85% methanol and 15% nitric acid. The potential was set at 20V and the temperature of the solution was maintained between -30°C and -50 °C. The Tenupol pump control flow rate was set at 5.0. Freezer storage of all samples at 0°C minimized further aging prior to examination under the TEM. A JOEL 100 CX transmission electron microscope operating at an accelerating voltage of 120V was used for all observations.

D. DIFFERENTIAL SCANNING CALORIMETRY (DSC)

The changes in energy associated with the precipitation or dissolution of second phase precipitates as a function of the temperature was measured using

the Perkin-Elmer Model 2C Differential Scanning Calorimeter (DSC). Thin sheets of approximately 15mm thickness were made using conventional machining techniques. Disks 5.5mm in diameter were cut from the sheets by electric discharge machining. All disks were sanded to approximately the same size and weighed on an analytical balance. The samples were heat treated in a vertical tube furnace with an argon purge and quenched by subsequently dropping them into an ice water bath. the solution treatment was performed at 530°C for 90 minutes. Immediately upon removing the samples from the quench bath they were dried and placed into the DSC. Three DSC runs were made for each sample to ensure reproducibility of results. All DSC runs started at 280°K ended above 700°K and were made with a constant heating rate of 10°C/minute. A pure aluminum sample, of approximately equal mass, was prepared from the DSC sample pan lids as the reference. The energy range setting for all runs was set at 10 mcal/second. A glove box with a nitrogen purge was necessary to minimize frost formation on the sample chamber. After a scan was completed the data was converted to heat capacity verse temperature. All heat capacities were compared to the heat capacity at 280°K by the following relation:

$$Cp \ Relative(T) = Cp(T) - Cp(280K)$$

In the alumina containing material (MMC), the DSC traces were normalized so they referred only to the mass of the aluminum matrix.

The important results obtained from the DSC for this report is the relative size of the peaks and position of the peaks relative to the temperature scale. The vertical shifts observed at the higher scanning temperatures are a result of the baseline shift between DSC runs. Repeatability of results, of relative peak size and temperature at peak, of multiple DSC scans demonstrate the accuracy of the equipment for the important aspects of this DSC analysis.

IV. RESULTS AND DISCUSSION

A. DIFFERENTIAL SCANNING CALORIMETRY

1. Characterization of the DSC Thermogram for the 2014 Aluminum Alloy.

Figure 3 shows the DSC thermogram of the 2014 aluminum alloy. The sample was solutionized for 1.5 hours at 535°C followed by an ice water quench. The calorimetry was performed with the following parameters.

- Heat Rate 10°C/min

- DSC Energy Range - 5mcal/sec

- Chart Recorder - 10 mV full scale

- Sample Size - 46 mg

Three exothermic formation peaks along with what appears to be a endothermic dissolution peak are observed in Figure 3. The exothermic peaks, corresponding to the formation of a new phase in the microstructure, are centered at 349K, 508K and 557K. The endothermic peak, corresponding to the dissolution of a phase present in the microstructure, is centered around 450K and is at least 60°C wide. This thermogram corresponds closely to the results presented by Abis and Riontino [Ref. 4].

33
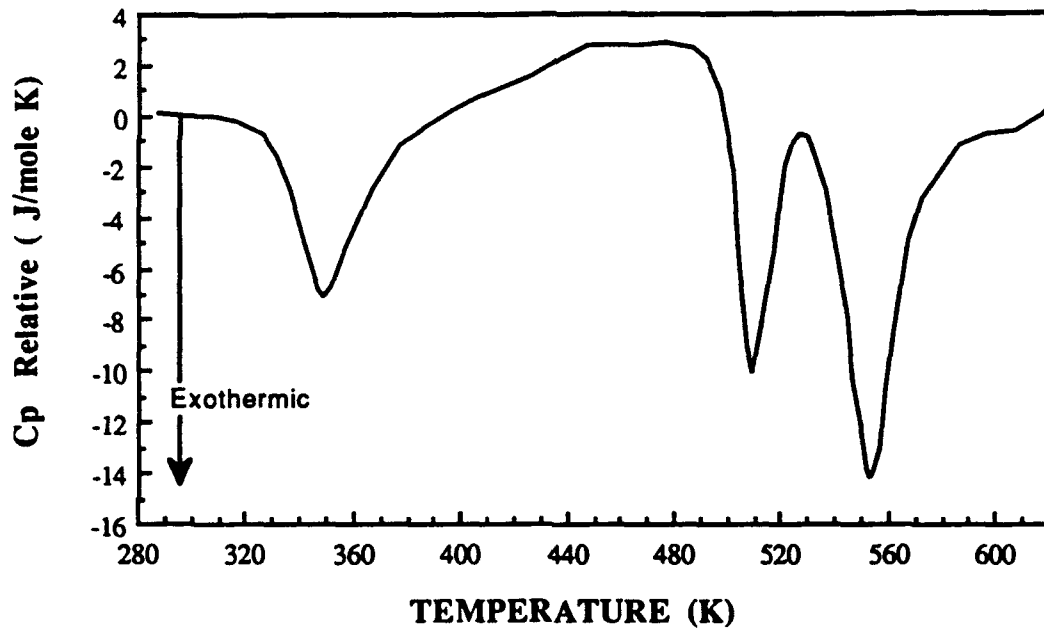
Figure 3: DSC Thermogram of solutionized and as quenched 2014 Al alloy.

Figure 4 shows the superimposed thermogram of the aluminum alloys 2014, 2024 and Al-4%Cu. This comparison was done in an attempt to positively identify the three formation peaks which take place in the 2014 Al alloy. The Al-4%Cu alloy was chosen because it is well known to form the θ phase sequence of precipitates ($CuAl_2$) [Refs. 17, 26]. The aluminum alloy 2024 was chosen because it has been shown to form the S phase sequence of precipitates ($CuMgAl_2$) [Refs. 14, 17].

From Figure 4 it can be observed that the first peak, positively identified in the 2024 Al alloy as GPB formation [Ref. 17], matches very close to the first exothermic peak of the 2014 Al alloy. It is important to note the Al-
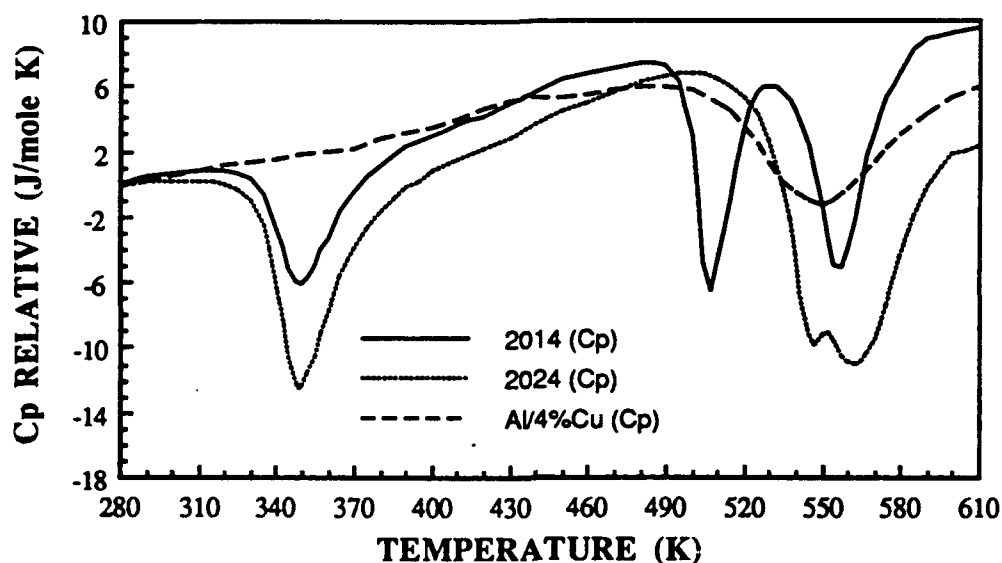
Figure 4: DSC Thermogram of the aluminum alloys; 2014, 2024 and Al/4% Cu.

4%Cu alloy does not show any phase activity in the temperature range of this first peak.

The peak identified as S' [Ref. 17] in the 2024 Al alloy appears to match the 3rd exothermic peak of the 2014 Al alloy. The single exothermic peak of the Al-4% Cu alloy, which has been identified as θ' also appears to be centered in the region of the third exothermic peak of the 2014 Al alloy.

Figure 4 is strong evidence in support of the proposition that the first exothermic peak in the 2014 Al alloy signifies the formation of GPB zones. The comparison in Figure 4 of the second and third exothermic peaks in the 2014 Al alloy results in no conclusive evidence that can positively identify these

35

peaks, Information is obtained here that would suggest that the second and third peaks in the 2014 Al Alloy can be attributed to S' and θ' precipitation. Further investigation is necessary to positively identify the precipitation phases that are occurring in the region 480K to 580K.

Figure 5a is the TEM micrograph of the 2014 Al alloy after solutionizing and quenching. Coarse vacancy loops are visible throughout the microstructure. This would suggest that the silicon in this alloy is "tied up" elsewhere in the microstructure since silicon is known to have a high affinity for vacancies and thus prevents the formation of the vacancy loops. This is further supported by the identification of large quantities of Si and Mn by Energy Dispersive X-Ray Spectroscopy (EDX) (Figure 5b) in the second phase particles, one of which can be observed in the Figure 5a micrograph. These second phase particles persist throughout the DSC aging treatments and are assumed to be insoluble in the temperature range of this investigation.

The observation of the vacancy loops and the determination of large amounts of Si and Mn in these insoluble particles is important evidence that suggests the β phase sequence (Mg_2Si) is not a contributor in the age hardening of this alloy. This is suggested by Abis and Riontino [Ref. 4].

Figure 6a is the TEM micrograph of a 2014 Al alloy solutionized and heat treated in the DSC up to 360K to reveal the microstructure corresponding to the first exothermic peak. A "fine mottled structure" similar to that
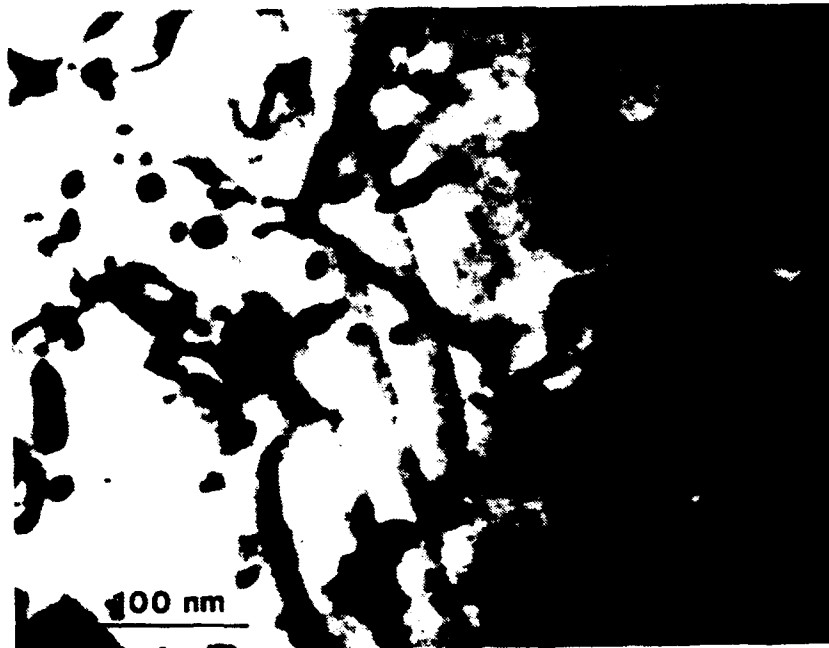
Figure 5a: TEM Micrograph of the 2014 Al alloy, solutionized and quenched, showing vacancy loops throughout the microstructure.
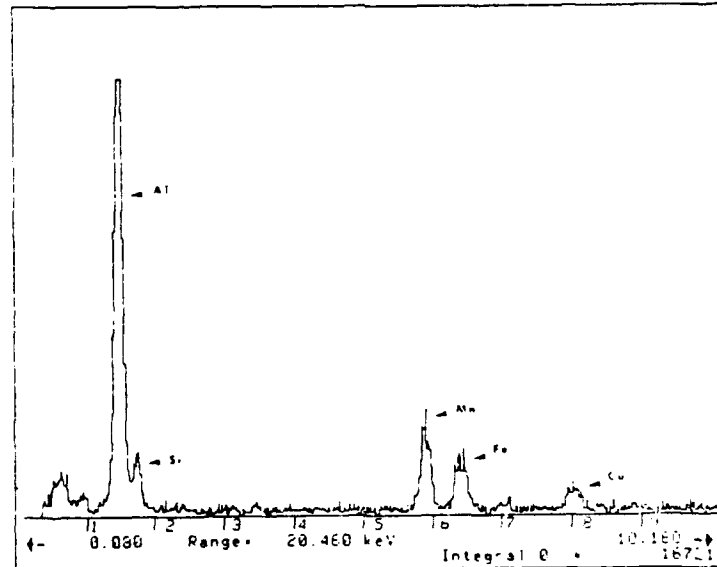
Figure 5b: EDX spectral analysis of the large insoluble particles found in the solutionized and quenched microstructure of Figure 5a.

37

identified as GPB zone effects by Bonfield and Datta [Ref. 5] can be seen in this micrograph.

The corresponding selected area diffraction pattern (SADP), Figure 6b does not reveal any streaking or diffraction spots representative of precipitate formation. This indicates that the precipitates must be fully coherent with the matrix and produce little well-defined strain fields. These characteristics are identical to those of GPB zones as reported by Datta [Refs. 5, 12] and Silcock [Ref. 11].

From the information obtained by TEM, SADP and the DSC Thermogram comparison (Figure 4), it can be concluded with some certainty that the first exothermic peak exhibited in the DSC thermogram (Figure 3) can be assigned the precipitation of GPB zones of the Al-Cu-Mg phase sequence.

Figure 7 is the TEM micrograph of the 2014 Al alloy heated in the DSC up to 510K at 10°C/min. to reveal the microstructure corresponding to the second exothermic peak. Observable in this micrograph are what appear to be three, specifically shaped, independent, second phase precipitates. Throughout the microstructure is a very fine, homogeneously dispersed precipitate of nearly spherical shape. The second precipitate observable is thin, needle shaped particles that are orientated in the [100] and [010] Al matrix direction. These needle-like precipitates appear to be randomly distributed throughout the microstructure. The third precipitate observed can only be found distributed on matrix dislocations and are needle shaped but with a much
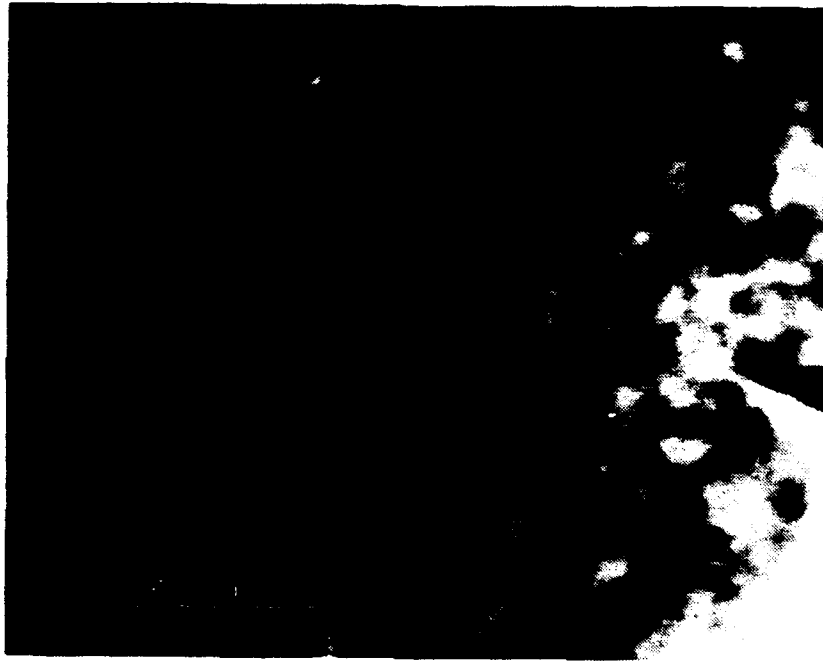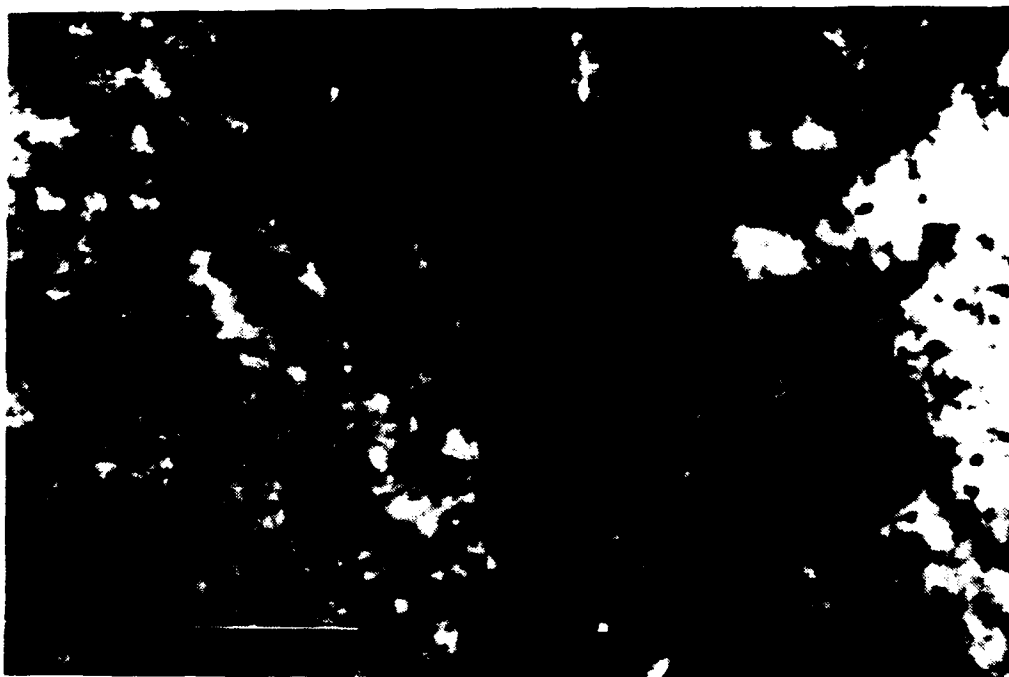
Figure 6a: Bright Field (BF) TEM micrograph of the 2014 Al alloy
              heated at 10°C/min. to 350K, which corresponds to the
              middle of the first exothermic peak.
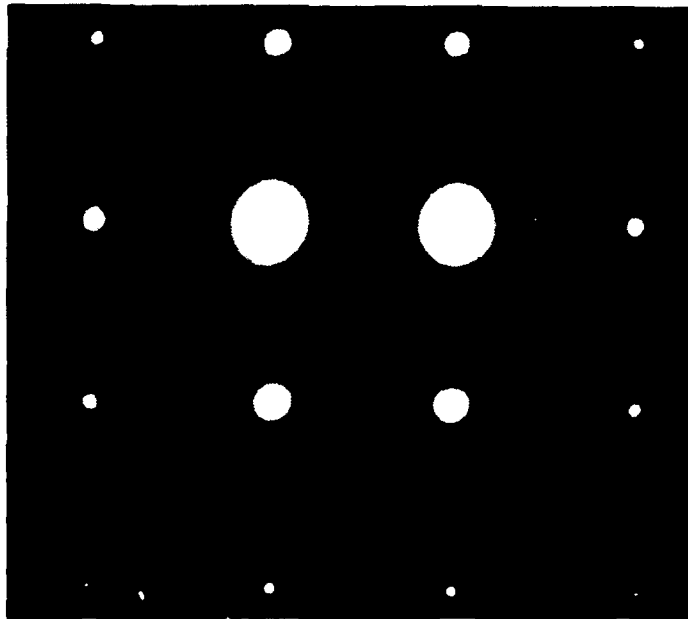
Figure 6b: The corresponding Selected Area Diffraction Pattern
              (SADP) of the 001 pole showing no features
              representative of precipitate formation.

39

Figure 7: TEM micrograph of the 2014 Al alloy, heated at 10°C/min. to 510K, which corresponds to the second exothermic peak.

wider cross section than the homogeneously dispersed needles. This second much larger diameter needle is oriented in the [100] direction. Additionally, there is only a few of the larger needle shaped precipitates found on the dislocations.

The fine, homogeneously dispersed needles and the dot-like precipitates are assumed to be the same phase with the end view of the needle giving the appearance of spherical shape. The precipitates in the body and the precipitates on the dislocations are assumed to be separate phases since only a few needles are seen on the dislocations whereas a large number of the thin

needles are observed throughout the body. Since precipitation is preferable at dislocations, if these were the same phase,there would be much more precipitates visible at the dislocations then what is currently observed.

From the assumption of two independent phases in this microstructure, identification of the second exothermic reaction peak can be achieved if these precipitates can be identified. From DSC comparisons (Figure 4) and the alloys composition, these two peaks should most likely be assigned to the precipitation of S' and θ'. This correlates with data from Abis and Riontino [Ref. 4] and Conserva *et al*. [Ref. 17].

The fine evenly dispersed needle shaped particles are most probably S' precipitates. This is in agreement with Wilson [Ref. 6] who found that the addition of small amounts of silicon to an Al-Cu-Mg alloy caused the precipitation of very fine S' needles in the [100] directions throughout the body of the matrix. This is further collaborated by Sen and West [Ref. 27] reporting on work done by Weatherly that silicon significantly slows the coarsening of S' and promotes the formation of a much finer precipitate throughout the matrix.

From observing the information about the second peak (DSC, TEM and other investigations) the larger needle shaped particles found on the dislocations should be assumed to be θ', which is known to prefer nucleation on dislocations [Ref. 24, 28]. But when combining this information with the information gleaned from the third peak, it becomes obvious that these

41

precipitates are part of the third exothermic peak which has been positively identified as θ'.

Figure 8 is the TEM selected area diffraction pattern (SADP) corresponding to the microstructure of Figure 7. Very faint <100> diffraction streaking through the {200} and {220} matrix spots is observable and is not reminiscent of any of the S phase sequence. This streaking should most probably be attributed to θ' [Ref. 28]. Diffraction spots in the 110 positions are very distinctive and can be noted along with some streaking from these spots. These spots are representative of the θ' phase. The faint streaking observed in the <100> direction through the matrix {100} and {110} positions can be attributed to either the S' or θ' phases and probably are resultant from the diffraction of both phases in the microstructure. The S' precipitate as reported by Silcock [Ref. 11] is only partially coherent with the microstructure and should cause only a small matrix strain, resulting in only faint streaking.

There are many things taking place in the temperature range of the second exothermic peak. This can be seen in the DSC trace and the TEM results. Because of partial superposition of the second and third peaks, a measurable amount of the phase forming at the second exothermic transformation peak may be attributed to the third exothermic peak. This may be further demonstrated by what appears to be at least two different phases observed in the microstructure. Another difficulty in defining this phase by SADP is the striking similarities between the S' and θ' diffraction patterns.
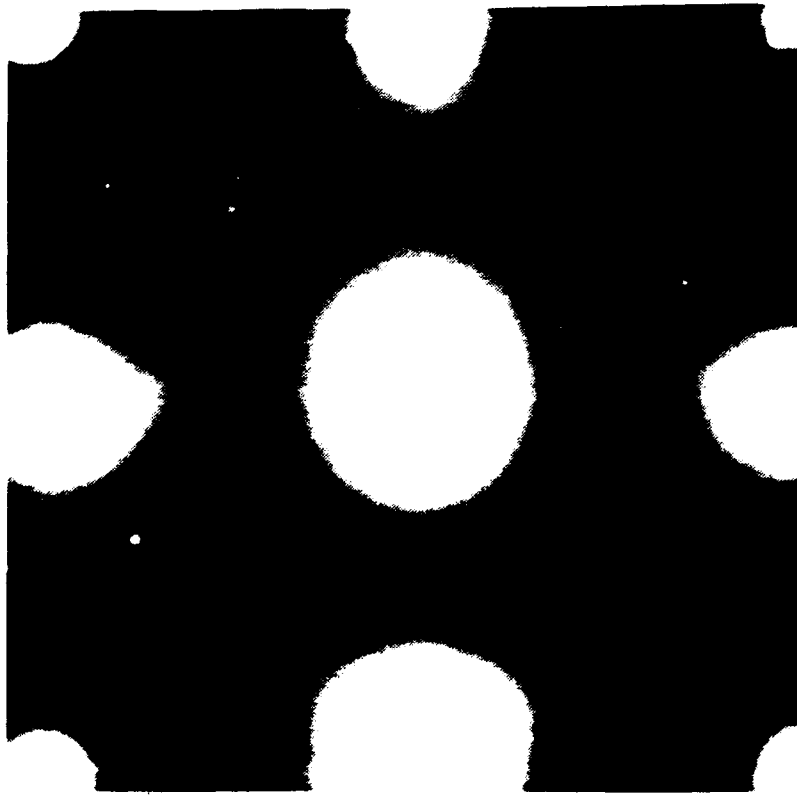
Figure 8:   Selected Area Diffraction Pattern (SADP) of the 001 pole corresponding to the micrograph of Figure 7.

The primary difference between these two patterns is the easily discernable 110 diffraction spots which is a characteristic of the θ' and not the S' pattern. If the θ' and S' are both present in the matrix the θ' diffraction spot at the 110 location would positively prove θ' presence but the presence of S' could not be proven. This could be what is happening in this alloy.

The results obtained via the alloy's DSC comparison (Figure 4) the TEM micrograph corresponding to the second exothermic peak (Figure 7), the alloy composition with the phases potentially possible in this alloy, together

43

with the fact that GPB zones have formed, leads to the proposal that the second peak is due to S' precipitation. However, since the SADP (Figure 8) does not absolutely verify the existence of the S' phase, it is not currently possible to confirm this proposal. Other research by Abis and Riontino [Ref. 4] suggest similar results. Further research is necessary to positively identify the precipitate forming during the second peak.

The microstructure corresponding to the third exothermic peak can be seen in Figure 9a. Large needle like precipitates are seen to have formed on dislocations. These precipitates have coarsened significantly and are more rod like than needle shaped. Their numbers have also increased significantly. The SADP of the microstructure at the third DSC peak can be seen in Figure 9b. The diffraction characteristics positively identify this phase as θ' as determined by Papazian [Ref. 26].

In summary it is proposed that the first exothermic peak can be attributed to the precipitation of GPB zones which are homogeneously distributed throughout the matrix. The second exothermic peak has not been positively identified but is possibly due to S' precipitates. The third exothermic reaction is attributed to the formation of θ' precipitates which nucleate specifically on dislocations.
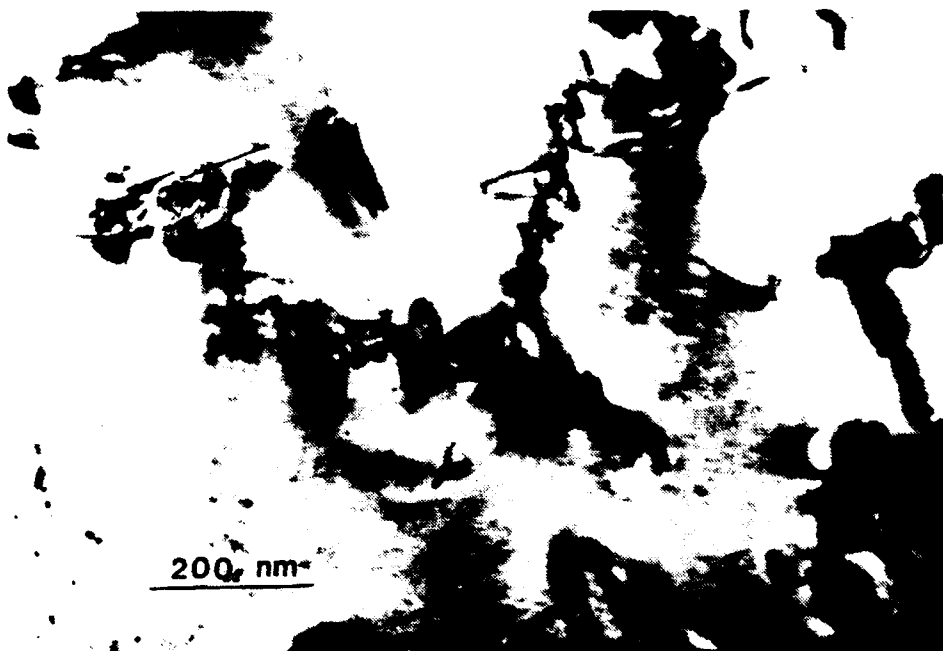
Figure 9a: Bright Field (BF) TEM micrograph of the 2014 Al alloy, heated at 10°C/min. to 560K, which corresponds to the middle of the third peak.
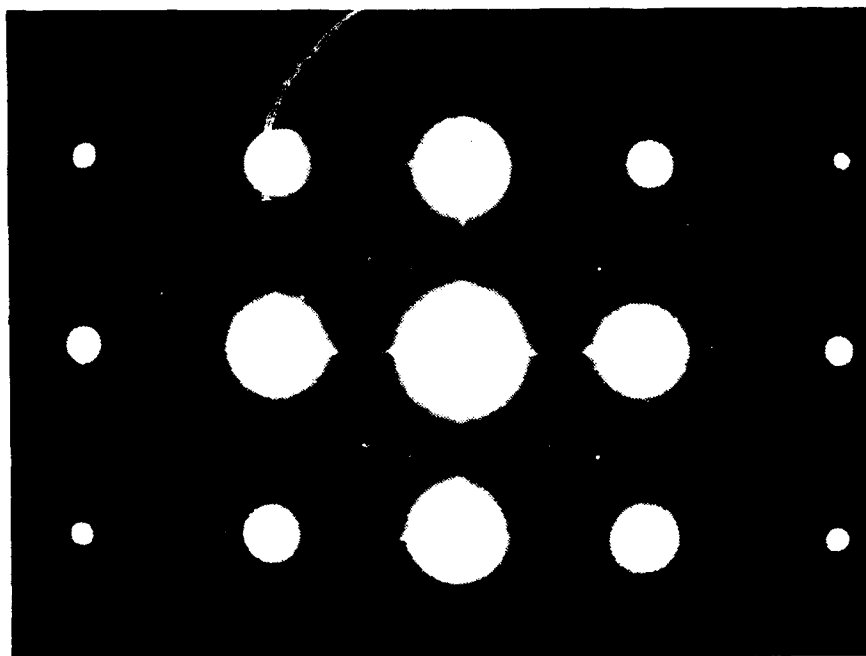
Figure 9b: The corresponding SADP of the 001 pole from the microstructure of Figure 9a.

2. Effects of Alumina Reinforcement Addition on the Matrix Precipitation Sequences

Results from the DSC scans of the 2014 Al alloy, the 2014 10 vol% Al_2O_3 MMC and the 2014 15 vol% Al_2O_3 MMC are shown in Figure 10. All DSC curves were normalized so they refer only to the mass of the aluminum alloy matrix. The aspects of interest of these DSC results are the locations of the reaction peaks on the temperature scale and their relative size. The relative size of the peak gives the reaction enthalpy which is directly related to the volume fraction of the precipitating phase. The temperature of the peak reaction rate is related to the size and stability of the precipitate [Ref. 28].

There are several distinct features that can be observed in Figure 10. Peak formation temperature and the relative area of the peak is affected, in some way, at all three precipitate formation peaks. In order to better compare the corresponding formation peaks Figure 11 and Figure 12 are included for discussion.

The effects of 10 and 15 vol% alumina addition on the GPB zone formation peak can be seen in Figure 11. From this figure it can be determined that the formation of GPB zones occurs at a slightly lower temperature in the MMC materials than in the monolith. This demonstrates that formation of GPB zones is accelerated in this alloy with the addition of the Al_2O_3 reinforcement. There is a pattern developed here where a continual decrease

46
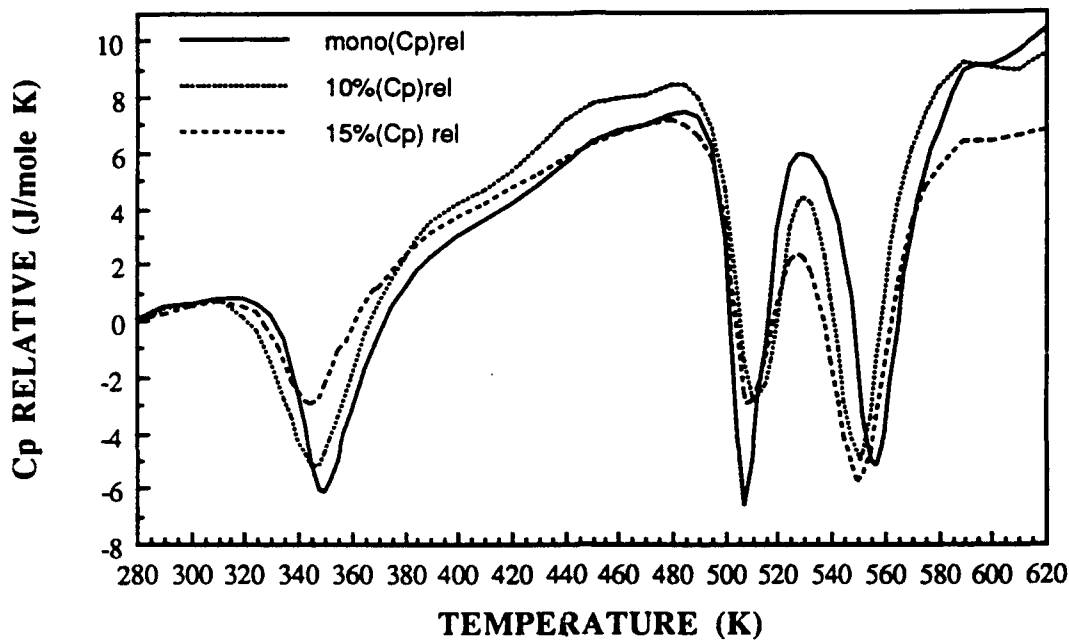
Figure 10:   DSC Thermogram of 2014 Al alloy reinforced with 0, 10, and 15 vol% Al₂O₃.

in peak temperature is obtained as the amount of alumina reinforcement is increased.

Accelerated aging is generally attributed to either enhanced dislocation density or an enhancement of the diffusion path. GPB zone formation requires only short range diffusion and is therefore not a diffusion dominated process. The dislocation density increases significantly with the addition of 10 vol% alumina reinforcement but only a slight difference in the dislocation density has been observed between the 10 vol% alumina and 15 vol% alumina reinforcements [Ref. 15]. The acceleration of the GPB zone formation is significant for the 10 vol% MMC but the additional 5 vol%

47
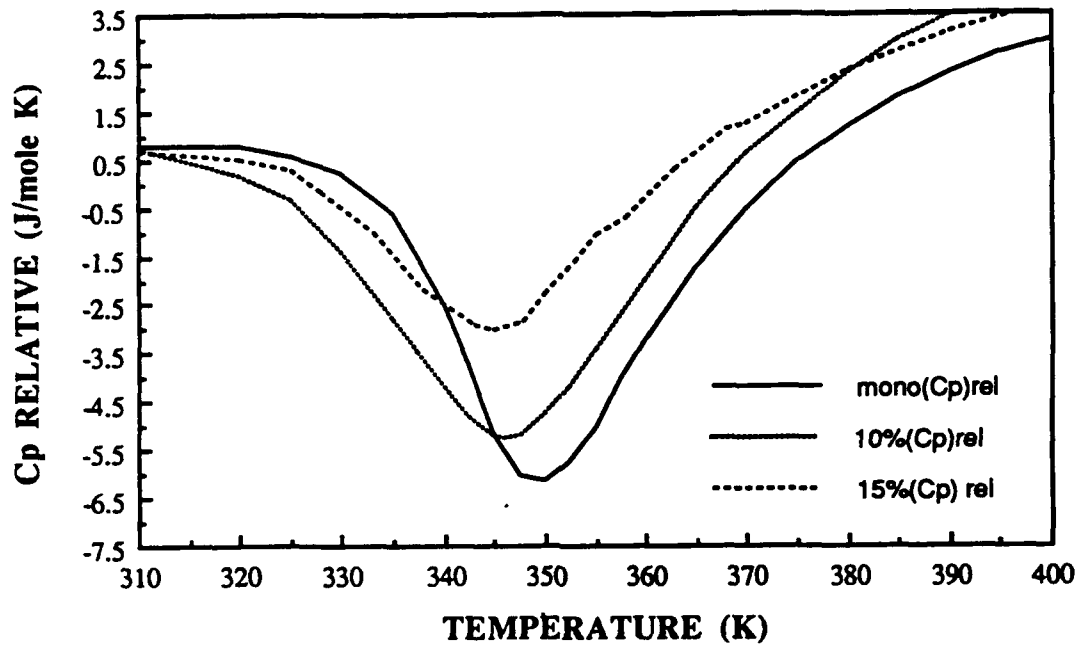
Figure 11: **Enlargement of Figure 10 to enhance the observation of the effects of the alumina addition on GPB zone formation.**

reinforcement in the 15 vol% MMC further accelerates the formation peak only slightly. This behavior matches with the increases in dislocation density and therefore the accelerated precipitation of the GPB zones can most probably be attributed to the enhancement of the dislocation density in the MMC.

The relative size of the GPB formation peak is directly proportional to the volume fraction of precipitates formed. It can be observed here that as the volume percent of alumina reinforcement increases the relative amount of GPB zones that precipitate during the DSC scan decreases.

48

It is observed from the analysis of the electrical resistivity measurements for an isothermal aging temperature of 317K that the enhanced dislocation density causes the formation of GPB zones after a very short incubation period, which is observed to be much longer in the monolith. This suggests the probable reason for the reduced GPB peak size in the MMC is due to some zones forming prior to the DSC scan, reducing the solute and nucleation sites available for GPB zone formation during the scan.

Additionally, because the 10 vol% MMC tends to have more clustering of reinforcement than the 15 vol% MMC there are larger matrix areas where the effects of the reinforcement should be minimal. These areas would have a proportionately larger amount of solute available for GPB zone formation during the DSC scan, and thus would enlarge the formation peak of the 10 vol% MMC. This would explain why the 10 vol.% MMC does not exhibit as much of a decrease in GPB zone peak size relative to the 15 vol.% MMC.

The results of the addition of alumina particle reinforcement to the formation of the second peak and θ' precipitates can be seen in Figure 12. A comparison of the second DSC peaks of the monolith and the two MMC's results in the observation that the addition of the alumina reinforcement apparently delays the precipitation of the second peak. The precipitates formed during the 2nd peak appear as the long thin needles observed in Figure 7. If this second peak is indeed due to the precipitation of S' as the number of

Figure 12: **Enlargement of Figure 10 to enhance the observation of the effects of the alumina addition on the formation of the 2nd peak precipitates and θ' precipitates.**
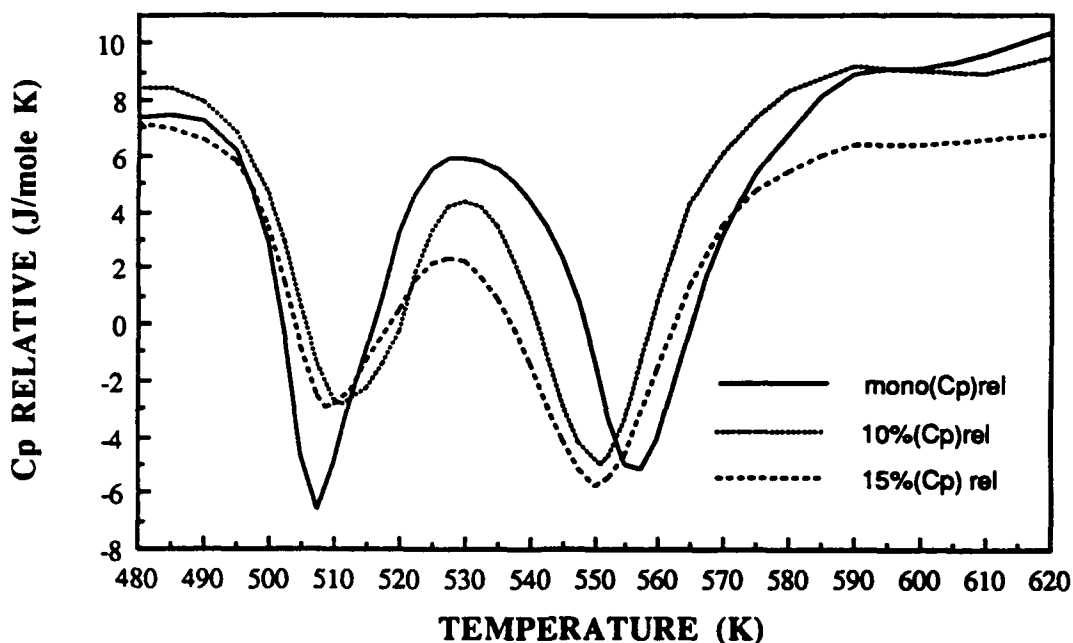
dislocations increase, there is a decrease in the number of GPB zones and nucleation sites for S' in the matrix.

The θ' precipitates have been observed to nucleate on dislocations. The precipitation of S' and θ' both require copper atoms and are therefore competitive processes. As the θ' precipitation is enhanced by the addition of dislocations the S' precipitation must be affected. This effect of enhanced θ' formation is visible by the higher temperature required for the peak reaction formation of S'.

Alternatively the increase in the peak reaction formation of the second peak precipitates may be affected not because their reaction kinetics are changing but because this peak is also partially the effect of the third peak (θ' formation) and the formation of θ' has been significantly affected by the reinforcement addition. The accelerated aging is significant in the third peak identified as θ'. Additionally this peak has substantially broadened as a result of the alumina addition. The third peak (θ') begins at a lower temperature in the MMCs, and hence the degree of superposition of the second and third peaks is greater in the MMCs. This might cause the apparent shift of the second peak to higher temperatures in the MMC. Therefore it is quite possible that a significant portion of the apparently delayed nucleation of the second peak precipitates, is not due to a change in their formation kinetics but due to the accelerated kinetics of θ' formation. If indeed this second peak is due to S' precipitation, this would more closely fit the results of the investigation by Papazian [Ref. 22]. He found that the formation kinetics for S' were not affected at all by the addition of SiC whiskers in an Al-Cu-Mg alloy. Although another possible reason for the differences between Papazian's results and this present study is that his alloy ratio was such that the $CuAl_2$ (θ) phase sequence was not kinetically favored therefore the S' formation was not competing for copper atoms with θ', as appears to be the case in the 2014 Al alloy. Although the two proposed reasons for delayed nucleation of the second

peak were discussed separately it appears that they both play a part in the total effect.

The effects of the addition of alumina particles on the aging kinetics of the third DSC peak, corresponding to θ' formation, can be seen as the peak occurring at the higher temperature in Figure 12. The alumina reinforcement has caused substantial acceleration of the θ' precipitation. This is the direct consequence of the increased dislocation density. The alumina reinforcement addition causes a substantial increase in the dislocation density. The θ' precipitate was observed to form on dislocations (Figure 7). This preferential attraction to dislocations as nucleation sites combined with the highly enhanced dislocation density, results in the observed accelerated precipitation of θ'. Because the magnitude of change in dislocation density between the two MMCs is relatively small, there is no noticeable effect of the additional 5% alumina in the 15 vol% MMC. This is in agreement with Suresh et al. [Ref. 23] who observed no difference in the accelerated aging effects of 6 vol% and 20 vol% SiC particles in a Al-4%Cu alloy.

Table II is a summary of the temperatures at which each of the DSC phase transformations peak, for the 2014 Al alloy with 0, 10, and 15 vol% alumina additions.

TABLE II. DSC PHASE TRANSFORMATIONS PEAK TEMPERATURE

Tp	0% A$_2$O$_3$	10% Al$_2$O$_3$	15% Al$_2$O$_3$
GPB zones	349K	346K	345K
2nd Peak Precipitates	507K	510K	509K
θ'	557K	551K	552K

B. THE EFFECTS OF ALUMINA ADDITIONS ON THE ARTIFICIAL AGING CHARACTERISTICS OF THE 2014 Al ALLOY

1. Electrical Resistivity

The variation in electrical resistivity with isothermal aging at temperatures of 40°C, 100°C, 150°C, and 200°C was measured and the results are presented here. The variation in resistivity accompanying aging can be grouped into three broad categories or zones.

- Zone 1 consists of the initial, usually rapid, rise in resistivity.

- Zone 2 follows Zone 1 and is characterized by a leveling off of the resistivity with very little change during continued aging.

- Zone 3 follows Zone 2 and represents the overaging of the precipitating phases. The electrical resistivity starts to drop off and is further reduced upon continued aging.

The electrical resistivity changes that occur due to aging, be it natural or artificial, correspond to many complex microstructural changes that may occur simultaneously. Several possible microstructural changes that contribute to the change in electrical resistivity include ; (1) vacancy formation

53

and absorption, (2) solute atoms going into, or coming out of, solution, (3) formation of precipitates with sizes comparable to an electron wavelength, (4) clustering of solute atoms and (5) changes in the size and boundaries of precipitate zones and dislocation structures [Ref. 14]. Basically any microstructural change that affects the scattering of conduction electrons will affect the electrical resistivity.

The initial rise in resistivity is usually attributed to the formation of small solute rich zones, which because of their critical size relative to an electrons wavelength, significantly scatter conduction electrons, thus raising the material's electrical resistance.

The peak in electrical resistance is usually attributed to the completion of this zone formation and the start of dissolution of these zones back into the matrix or transformation of these zones into a second less coherent phase. The small changes in resistivity occurring here can be attributed to the decrease in resistivity caused by the removal of the solute atoms from solid solution balanced by the slow precipitation of additional solute rich zones [Ref. 15] causing an increase in resistivity.

The decrease in resistivity which is labeled Zone 3 is the result of the coarsening of the small zones into precipitates that now have a size substantially greater than the conduction electrons wavelength. This increased precipitate size is therefore less effective at electron scattering. Another effect of the coarsening on electrical resistivity is the continued removal of solute

54

atoms from the solid solution. As the solute atom density in the sold solution decreases the resistivity also decreases. Additionally as coarsening occurs, these zones transform from coherent to semi-coherent precipitates, reducing the strain fields around the precipitate and thereby reducing the efficiency of the precipitate in scattering electrons.

Resistivity measurements of the monolith and two MMCs aged at 200°C can be observed in Figure 13. All three material's exhibit exactly the same shape but with varying magnitudes of resistivity change. This fact along with nearly equivalent times to peak and to the inflection points demonstrates that the same precipitates and phase sequences are taking place in all three of these materials but with varying volume fractions of each. The difference in magnitude should be explained on the basis of a difference in the volume fraction of the matrix material in each sample. These samples were all the same size but the monolith is made of 100% 2014 aluminum, while the 10 vol% and 15 vol% alumina MMCs have 86% and 79% by weight, 2014 aluminum respectively. Less matrix material corresponds to less material available for phase transformation. This can not, however, account for all of the difference in these resistivity plots and therefore there must also be a difference in the amount of second phase precipitation that takes place due to the alumina addition. This is readily observable in Figure 13 at the peak, where the amount of precipitation in the monolith is significantly greater than in the 10
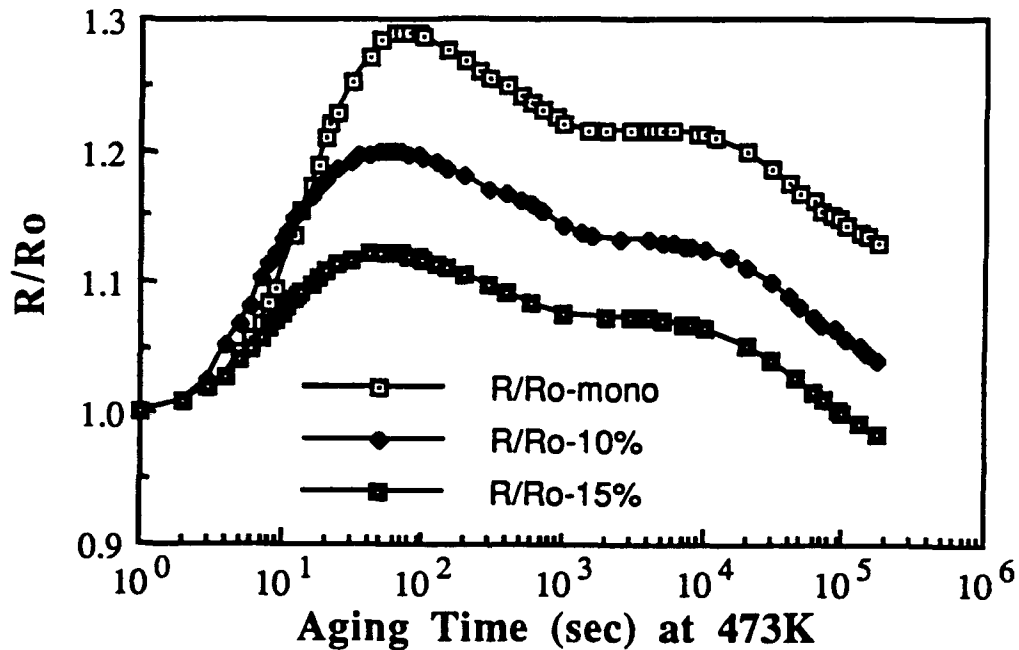
Figure 13: Changes in resistivity of 2014 Al alloy reinforced with 0, 10, and 15 vol% Al_2O_3 as a function of time at aging temperature.

vol% MMC. This difference is even more noticeable in comparison to the 15 vol% MMC.

In Figure 14 the changes in resistivity of the control alloy and two MMCs for aging at 150°C is presented. All three curves have similar shapes and transition times which signifies similar phases and precipitation sequences are taking place. The first large peak observed in the materials aged at 200°C is less prominent. The total change in resistivity has significantly decreased for the material aged at the lower temperature. The times to peak and to overaging have not significantly changed.
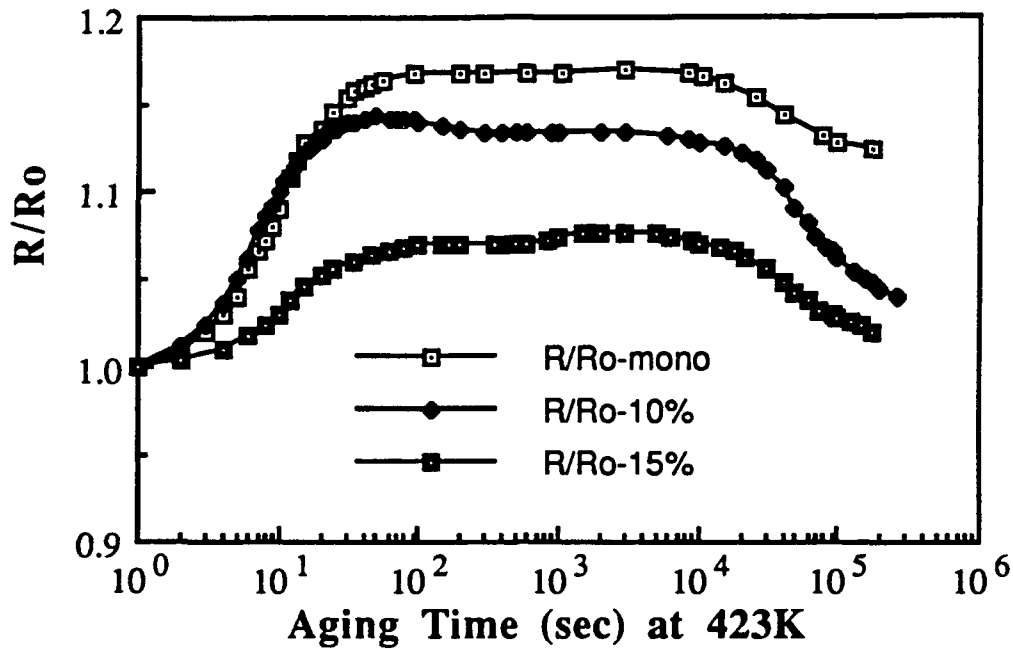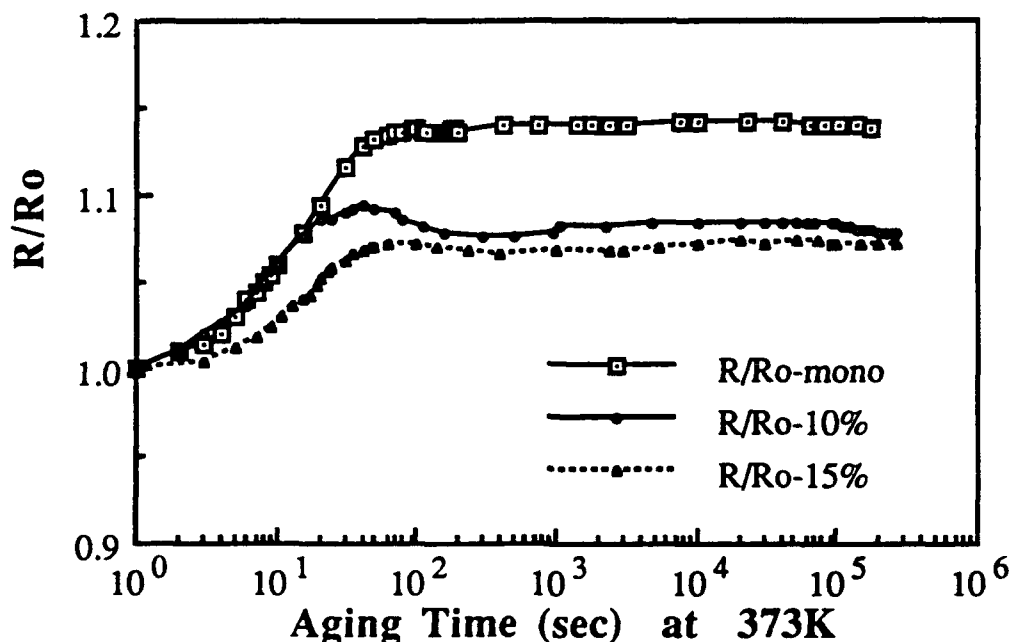
Figure 14: **Changes in resistivity of 2014 Al alloy reinforced with 0, 10, and 15 vol% Al_2O_3 as a function of time at aging temperature.**

Figure 15 shows the results of the tests conducted at an artificial aging temperature of 100°C. All three materials show basically the same phase sequences are taking place within the materials but there does appear to be some variance right after the peak is reached in the 10 vol% MMC. Although the time to peak has not significantly been altered the time at peak has grown substantially as the aging temperature is decreased to 100°C. No decrease in resistivity was observed even after 88 hours of aging at this temperature.

The electrical resistivity aging sequence for aging at 100°C, 150°C and 200°C can be explained as follows; As GP1 and GPB zones precipitate, the

decrease in the electron scattering that takes place due to the removal of solute

atoms (Mg,Cu) in the solid solution is small compared to the large increase in

the electron scattering due to the rapid increase in the number of GP1 and

GPB zones. Therefore as the GP1 and GPB zones precipitate, the electrical

resistance increases at its highest rate.

Figure 15: **Changes in resistivity of 2014 Al alloy reinforced with 0, 10, and 15 vol% Al$_2$O$_3$ as a function time at aging temperature.**

As aging continues the time required for incubation of θ" and θ', is

reached and these phases start to nucleate at the expense of the GP1 and GPB

zones. At 200°C it is evident that dissolution of the GPB and GP1 zones starts

prior to any significant nucleation of θ" and θ'. These larger precipitates grow

beyond the size that corresponds to the wavelength of the electrons, thereby scattering electrons less efficiently. Eventually the reduction of the electron scatter caused by the reduced number of copper and magnesium atoms in solid solution along with the coarsening of the precipitates will more than offset the increase caused by further nucleation. When this happens the electrical resistivity starts to decrease and will continue with further aging.

Figures 16 and 17 are TEM micrographs of the 2014 Al alloy aged at 200°C for 300 and 10,000 seconds respectively. Figure 16a is the micrograph corresponding to the condition right after the first resistivity peak, which can be observed in Figure 13. This microstructure closely resembles the microstructure of the second DSC peak (Figure 7). The SADP (Figure 16b) is similar to that of the second DSC peak but has some additional streaking in the <100> direction which is representative of GP1 zone formation [Ref. 5]. In addition, the 110 diffraction spot is significantly less distinct indicating less θ' present. Figure 17a is the micrograph corresponding to the end of the plateau observed in Figure 13. The SADP (Figure 17b) identifies these precipitates as θ' and θ''. Since the θ'' characteristic <100> streaking through the {200} and {220} spots are quite distinct, it appears that a significant amount of θ'' is present in this microstructure.

The effects of isothermal aging at 40°C on electrical resistivity can be seen in Figure 18. Three distinct differences can be observed when comparing the plots for aging above 100°C to this plot. The first observed
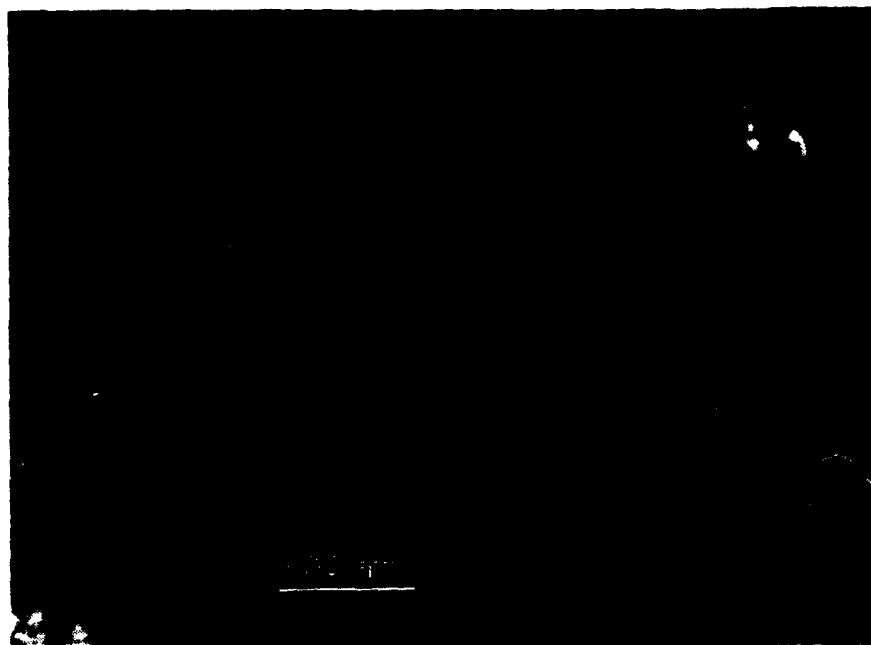
Figure 16a: Bright Field (BF) TEM micrograph of the microstructure of the 2014 Al alloy isothermally aged at 200°C for 300 seconds.
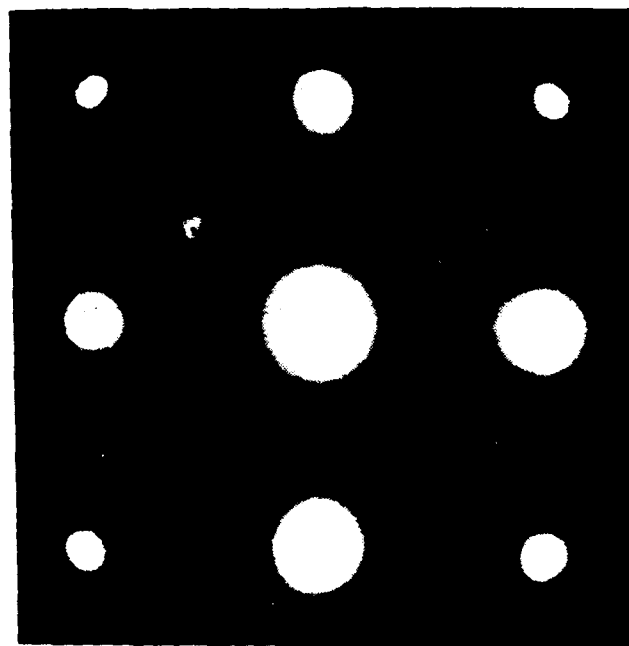
Figure 16b: The SADP of the 001 pole, corresponding to the microstructure of Figure 16a.
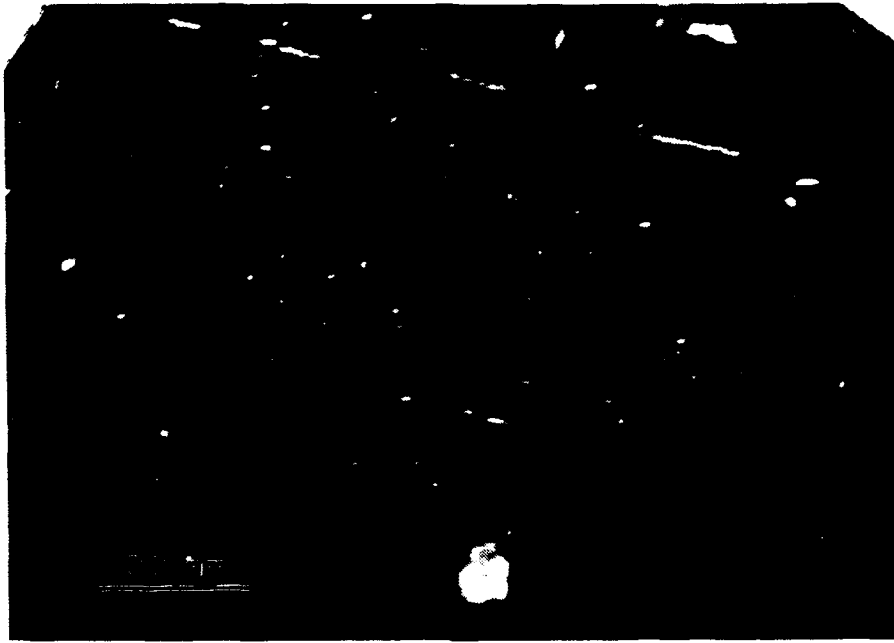
Figure 17a: Bright Field (BF) TEM micrograph of the microstructure of the 2014 Al alloy during isothermal aging at 200°C for 10,000 seconds.

Figure 17b: The SADP of the 001 pole, corresponding to the microstructure of Figure 17a.

61

difference is that no overaging is observed, even after eleven days of aging. This demonstrates that GPB and GP1 zones are relatively stable at this temperature. This is in agreement with the results of Rosen *et al.* [Ref. 14].
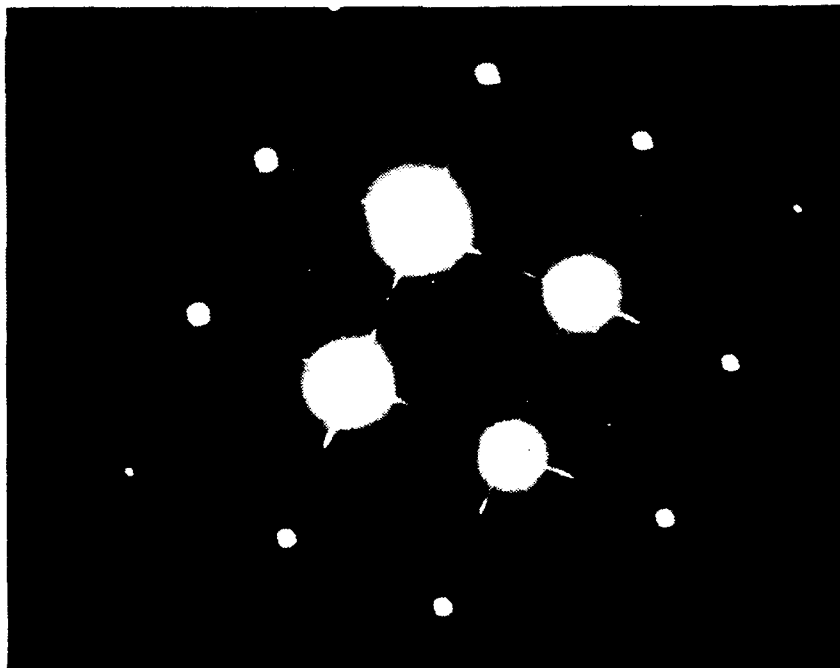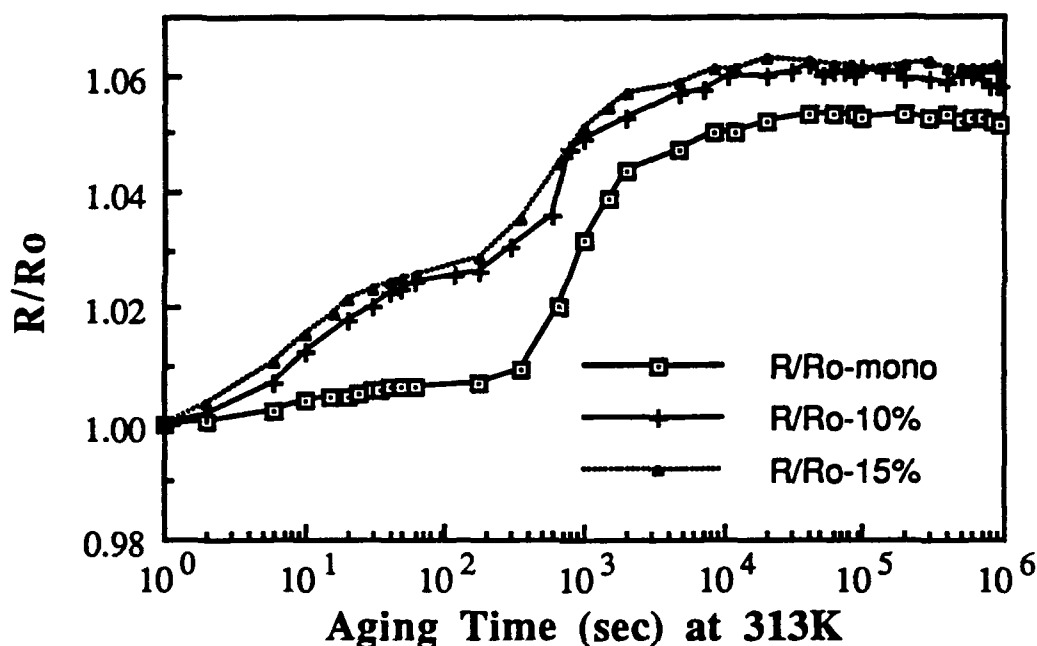

Figure 18: **Changes in resistivity of 2014 Al alloy reinforced with 0, 10, and 15 vol% Al$_2$O$_3$ as a function of time at aging temperature.**

The second observed difference in aging at 40°C compared to aging at and above 100°C is the much slower precipitation of GP1 and GPB zones. This hundredfold increase in aging time would suggest that the diffusion of the solute atoms has significantly decreased and the critical size of the nucleating precipitates must be substantially larger than the available local solute concentration.

The third difference between the higher aging temperatures and this aging temperature is a significant change in the effects of the reinforcement on the aging kinetics of the matrix. Only at this lower temperature has there been an increase in the rate of precipitation and the amount of precipitates formed in the alumina reinforced alloy.

The accelerated resistivity change observed in the MMC in Figure 18 can most probably be attributed to enhancement of the GPB zone formation due to the increased dislocation density. This acceleration of the GPB zone precipitation was also observed in the DSC results of the first exothermic peak (Figure 11).

2. Hardness Testing

Figure 19 shows the results of the hardness testing of the 2014 Al alloy with 0, 10 and 15 vol% Al_2O_3 additions. There are several observed effects of the alumina particle addition on the age hardening characteristics of the matrix.

Observation of the matrix microhardness in the solutionized and quenched condition reveals the two MMCs have a higher hardness than the monolithic 2014 Al alloy. This indicates that the enhanced dislocation densities, which are a result of the thermal expansion mismatch, contribute significantly to the strength at the beginning stages of aging. This is in disagreement with Suresh *et al.* [Ref. 23] but is in agreement with the bulk of literature in this area [Refs. 8, 10, 15, 25, 29].

63
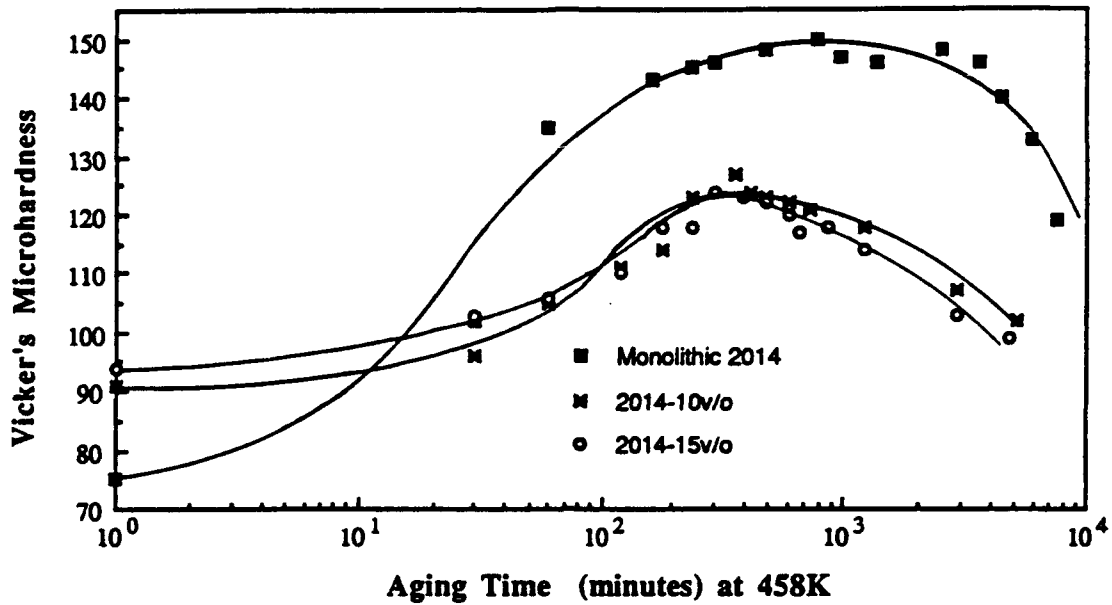
Figure 19: **Comparison of matrix microhardness for the 2014 Al alloy and two MMCs (10 and 15 vol% alumina) during isothermal aging at 185°C.**

The comparison of peak hardness and change in hardness from the quenched condition to the peak aged condition, indicates that the addition of alumina reinforcement significantly decreases the microstructural age hardenability of this alloy. The peak matrix hardness for both the 10 vol% and 15 vol% MMC is approximately 125VHN compared to a peak hardness in the monolith of approximately 150VHN. This effect is even more pronounced when comparing the change in hardness for the three materials. The monolith experienced a 75VHN increase to peak hardness, with isothermal ageing compared to a 30VHN increase in the two composite materials.

64

The decease in peak microstructural hardness is in variance with most literature available on the effects of reinforcement on the matrix hardenability. Specifically higher peak aging is attributed to more nucleation sites for the strengthening precipitate to form and therefore a larger number of second phase particles to block dislocation motion. However in the study by Christman and Suresh [Ref. 24] no appreciable difference in peak hardness was observed for a Al-Cu-Mg alloy with and without reinforcement.

Sen and West [Ref. 27] studied how the introduction of dislocations by mechanical deformation of a 2014 Al alloy affected the microstructural development at peak ageing conditions. Results indicated that even small amounts of deformation caused the preferential nucleation of θ' at the expense of θ''. θ' was found to heterogeneously nucleate at dislocations and θ'' was almost completely absent in the matrix that underwent deformation. For their control condition, 2014 Al with no deformation history, θ'' was found to be the principal hardening precipitate. Similar results were achieved by Gronostajski and Tobota [Ref. 10]. From this work it can be concluded that introducing dislocations into the microstructure of a 2014 Al alloy will cause the preferential nucleation of θ' at the expense of θ''.

The SADP for the 2014 Al alloy aged for 10,000 seconds at 200°C (Figure 17), indicates that the precipitate in the microstructure at this aging time is principally θ''. This corresponds to a point on the hardness plot (Figure 19) where the microstructure has reached over 95% of its peak hardness

condition. This indicates that θ'' is the primary contributor to the age hardening of the 2014 Al alloy. This is in full agreement with Singh and Goel [Ref. 8].

The addition of alumina to an aluminum matrix is known to cause a significant increase in the dislocation density [Ref. 15]. The increased density of dislocations provide additional nucleation sites for θ'. θ' and θ'' are thought to be competitive, vice sequential, nucleation processes [Ref. 27]. These three factors provide adequate information for explaining the lower peak hardness experienced in the composite matrix. The addition of the reinforcement to the alloy causes a substantial increase in dislocation density. θ' is preferentially nucleated at the expense of θ'' at these dislocations. The θ' which is semicoherent with the matrix, is not as effective a matrix strengthener as θ'' which causes larger strains in the matrix due to its fully coherent nature. Finally the small difference in the dislocation density of the two MMCs is not sufficient to noticeably affect the peak hardness of the matrix, when comparing the 10 vol% and 15 vol% MMC.

The third noticeable change in the microhardness measurements between the monolith and the composites is the aging time required to reach peak hardness. The two MMCs exhibit accelerated aging to the peak hardness condition. Peak hardness for the monolith is obtained after approximately 10 hours of artificial aging compared to approximately 4-5 hours for the two composites.

Finally, there was a good deal of data scatter in the composite measurements relative to the monolith. This is a good indication that the microstructure of the composite material is not as uniform as the monolith. It is possible in the regions where the alumina reinforcement is clustered, there is a measurable difference in the hardness compared to the rather large reinforcement free areas that were required for data collection. Care was taken to minimize this by varying load size and taking measurements as close to the reinforcement as the equipment would practically allow.

V. CONCLUSIONS

1. The age hardening sequence in the 2014 Al alloy as evaluated by DSC, can most probably be attributed to: 1) GPB zone formation at approximately 349K, and 2) θ' formation at 557K. In addition there is evidence that would suggest that the second exothermic peak can be attributed to S' formation at 507K.

2. The basic age-hardening sequence in the 2014 Al alloy is similar to the 2014 Al alloy reinforced with Al_2O_3 particulate.

3. The addition of the alumina reinforcement to the 2014 Al alloy matrix significantly affects the precipitation behavior. The effect of the alumina reinforcement, on the DSC phase transformation peak temperatures can be seen in Table II.

The addition of the Al_2O_3 reinforcement causes acceleration of the GPB zone nucleation kinetics with only a small difference in the transformation temperature between the two MMC.

The formation kinetics of the phase corresponding to the second DSC peak were delayed in the MMC relative to the monolith material. This is believed to be due to a combination of effects caused by the acceleration of θ' formation, which competes with the formation of the second exotherm (probably due to S').

The θ' formation kinetics are significantly accelerated in the alumina containing 2014 MMC, relative to the monolithic material. This is a direct consequence of the increased dislocation density in the MMC since these dislocations are the observed nucleation sites for this phase.

4. The overall aging behavior of the 2014 Al alloy is accelerated in the Al_2O_3 reinforced MMC relative to the monolithic material. The age hardenability of the 2014 Al alloy is significantly lowered by the addition of the Al_2O_3 reinforcement. These two effects of the alumina addition are explained by the formation of θ' in the MMCs. The increase in the dislocation density in the MMCs increases the nucleation sites for θ' accelerating its formation. The two phases θ' and θ'' are competitive nucleation processes and therefore the increase in the formation of θ' is at the expense of the θ'' formation. θ'' was found to be the primary hardening phase in the monolithic material. As the fraction θ''/θ' is decreased the hardenability of the alloy is also decreased.

5. The change is resistivity ($\Delta\rho$) increased with increasing aging temperature and this is attributable to the formation of a larger amount of coherent precipitates (GP1, GPB and θ'') at the higher aging temperatures.

6. Artificial aging at low temperatures exhibited accelerated aging and an increase in resistivity change ($\Delta\rho$) for the Al_2O_3 reinforced MMCs, relative to the monolithic alloy. This is probably due to an increased nucleation rate, leading to accelerated precipitation of GPB and GP1 zones.

LIST OF REFERENCES

1. Hunt, M., "Aluminum Composites Come of Age," *Materials Engineering,* Vol. 106, pp 37-40, January 1989.

2. Rohatgi, P., "Advances in Cast MMCs," *Advanced Materials and Processes,* Vol. 137, Issue 2, pp 39-44, February 1990.

3. Mills, K., *Metals Handbook,* 9th Edition, Vol. 2, ASM International, 1978.

4. Abis, S., Riontino, G., "Characterization of Commercial Tempers in High Strength Aluminum Alloys by Resistivity Technique," *Zeitschrift Fur Metallkunde,* Vol. 79, pp 202-205, 1988.

5. Bonfield, W., Datta, P.K., "Zone Formation during Room Temperature Aging of Al-4%Cu-.8%Si-.8%Mg," *Journal of Materials Science,* Vol. 12, pp 1050-1052, 1977.

6. Wilson, R.N., "The Effects of .24% Silicon upon the Initial Stages of Aging of an Aluminum - 2.5% Copper - 1.2% Magnesium Alloy," *Journal of the Institute of Metals,* Vol. 97, pp 80-86, 1969.

7. Bonfield, W., Datta, P.K., "Zone Formation During Room Temperature Aging of Al-4%Cu-.8%Si-.8%Mg," *Journal of Materials Science,* 12, pp 1050-1052, 1977.

8. Singh, D., Goel, D.B., "Influence of Thermomechanical Aging on Tensile Properties of 2014 Aluminum Alloy," *Journal of Materials Science,* 25, pp 3894-3900, 1990.

9. Paterson, S.J., Sheppard, T., "Structural Changes Occurring During Thermal Treatments during Extrusion of Al-Cu-Mg-Mn-Si (AA2014) Alloy," *Metals Technology,* Vol. 9, pp 389-398, October 1982.

10. Gronostajski, J., Tobota, A., "Thermomechanical Treatment of 2014 Aluminum Alloy," *Materials Science and Technology,* Vol. 4, pp 335-340, 1988.

11. Bonfield, W., Datta, P.K., "Precipitation Hardening in an Al-Cu-Si-Mg Alloy at 130 to 220°C," *Journal of Materials Science,* Vol. 11, pp 1661-1666, 1976.

12. Silcock, J.M., "The Structural Aging Characteristics of Al-Cu-Mg Alloys with Copper: Magnesium Weight Ratios of 7:1 and 2.2:1," *Journal of the Institute of Metals,* Vol. 89, pp 203-210, 1960.

13. Radmilovic, V., Thomas, G., Shiflet, G.J., Starke, E.A., "On the Nucleation and Growth of Al_2CuMg (S') in Al-Li-Cu-Mg and Al-Cu-Mg Alloys," *Scripta Metallurgica,* Vol. 23, pp 1141-1146, 1989.

14. Rosen, M., Horowitz, E., "The Aging Process in Aluminum Alloy 2024 Studied by Means of Eddy Currents," *Material Science and Engineering,* Vol. 53, pp 191-198, 1982.

15. Allen, S.M., "Effect of Alumina Particle Additions on the Aging Kinetics of 6061 Aluminum Matrix Composites," Master's Thesis, Naval Postgraduate School, Monterey, California, June 1990.

16. Dutta, I., Allen, S.M., Hafley, J.L., "Effect of Reinforcement on the Aging Response of Cast 6061 $Al-Al_2O_3$ Particulate Composites," Submitted for publication.

17. Conserva, M., DiRusso, E., Fiorini, P., "Aging and Structural Hardening Processes in Thermally Treated Aluminum Alloys," *Alluminio E Nuova Merallurgia,* No. 10, pp 515-532, 1970.

18. Van Den Brandt, B., Van Den Brink, P.J., Proceedings Second International Aluminum-Lithium Conference. 1983, TMS-AIME, Warrendale, Pennsylvania, 1983, pp 433-446.

19. Nieh, T.G., Karlak, R.F., "Aging Characteristics of B_4C- Reinforced 6061-Aluminum," *Scripta Metallurgica,* Vol. 18, No. 1, p. 25, 1984.

20. Christman, T., Suresh, S., "Microstructural Development in an Aluminum Alloy-SiC Whisker Composite," *Acta Metallurgica,* Vol. 36, No. 7, pp 1691-1704, 1988.

21. Dutta, I., Bourell, D.L., "A Theoretical and Experimental Study of Aluminum Alloy 6061-SiC Metal Matrix Composite to Identify the Operative Mechanism for Accelerated Aging," *Materials Science and Engineering,* Vol. A112, pp 67-77, 1989.

22. Papazian, J.M., "Effects of SiC Whiskers and Particles on Precipitation in Aluminum Matrix Composites," *Metallurgical Transactions A*, Vol. 19A, pp 2945-2953, December 1988.

23. Suresh, S., Christman, T., Sugimura, Y., "Accelerated Aging in Cast Al Alloy-SiC Particulate Composites," *Scripta Metallurgica*, Vol. 23, pp 1599-1602, 1989.

24. Christman, T., Suresh, S., "Microstructural Development in an Aluminum Alloy-SiC Whisker Composite," *Acta Metallurgica*, Vol. 36, No. 7, pp 1691-1704, 1988.

25. Hafley, J.L., "A Comparison of the Aging Kinetics of a Cast Alumina - 6061 Aluminum Alloy," Master's Thesis, Naval Postgraduate School, Monterey, California, December 1989.

26. Gerold, V., "On the St. .ctures of Guinier-Preston Zones in Al-Cu Alloys," *Scripta Metallurgica*, Vol. 22, pp 927-932, 1988.

27. Sen, N., West, R.F., "Some Factors Influencing S Precipitation in Al-Cu-Mg and Al-Cu-Mg-Ag Alloys," *Journal of the Institute of Metals*, Vol. 97, pp 87-92, 1969.

28. Papazian, J.M., "A Calorimetric Study of Precipitation in Aluminum Alloy 2219," *Metallurgical Transactions A*, Vol. 12A, pp 269-280, February 1981.

29. Vogelsand, M., Arsenault, R.J., Fisher, R.M., "An in Situ HVEM Study of Dislocation generation at Al/SiC Interfaces in Metal Matrix Composites," *Metallurgical Transactions A*, Vol. 17 A, pp 379-389, March 1986.